Sedimentary model for mixed depositional systems along the Pacific margin of the Antarctic Peninsula: Decoding the interplay of deep-water processes

S. Rodrigues [a,*], F.J. Hernández-Molina [a], R.D. Larter [b], M. Rebesco [c], C.-D. Hillenbrand [b], R.G. Lucchi [c], F.J. Rodríguez-Tovar [d]

[a] Department of Earth Sciences, Royal Holloway University of London, Egham, Surrey TW20 0EX, UK
[b] British Antarctic Survey, High Cross Madingley Road, Cambridge CB3 0ET, UK
[c] Istituto Nazionale di Oceanografia e di Geofisica Sperimentale, Borgo Grotta Gigante, Trieste 42/c 34010, Italy
[d] Departamento de Estratigrafía y Paleontología, Universidad de Granada, 18002 Granada, Spain

ABSTRACT

Mixed (turbidite-contourite) depositional systems are formed by a complex interplay of deep-water processes. An evaluation of their morphological elements and their lateral and spatial distribution is crucial to better understand the interplay of transport and depositional processes, involving along-slope bottom currents and down-slope turbidity currents. This work investigates extensive and still active mixed depositional systems developed along the Pacific margin of the Antarctic Peninsula, which comprise large asymmetric mounded drifts, dendritic channel-complex systems and wide trunk channels. These systems offer a unique setting to investigate diverse morphological elements at a high-resolution spatial scale (10–100 m), using multibeam bathymetry and acoustic sub-bottom profiles. Four main seismic units define distinct evolutionary stages for the Pleistocene to present day record: a) *1.3–1 Ma*, characterized by aggradational mounded drifts built by a dominant along-slope bottom current; b) *1–0.6 Ma*, built by synchronous interactions between a SW-flowing bottom current and NW-directed turbidity currents; c) *0.6–0.2 Ma*, characterized by deposition of thick gravitational deposits across the margin under a weak SW-flowing bottom current comprising modified Lower Circumpolar Deep Water (LCDW); and d) *0.2 Ma – present*, when synchronous interactions between the bottom current, characterized by flow speed fluctuations, and ephemeral turbidity currents led to intercalations of turbidites, contourites, reworked turbidite deposits and hemipelagites. Alternations in the stratigraphic stacking pattern suggest cyclic spatial and temporal variations of gravity-driven down-slope processes and along-slope bottom currents, which were responsible for the construction of these modern mixed depositional systems and which themselves were controlled by glacial-interglacial changes. The new results are compared with similar mixed depositional systems to decode the main processes involved in their formation, explore their interactions at short- and long-term time scales, and propose a conceptual sedimentary model.

1. Introduction

Along- and down-slope processes are key sedimentary and erosional processes in shaping most continental margins (e.g., Mosher et al., 2017). Along-slope bottom currents are considered persistent, long-term flows, while gravitational down-slope currents comprise ephemeral and rapid, sediment-laden flows. Their interaction can create large mixed (turbidite-contourite) depositional systems, which have been studied in detail during the last decade (Creaser et al., 2017; Fonnesu et al., 2020; Fuhrmann et al., 2020; Miramontes et al., 2020; Rodrigues et al., 2021).

The variable interplay between gravity and bottom currents primarily generates contourite-dominated mixed systems (Brackenridge et al., 2013, 2018; de Castro et al., 2020; Mencaroni et al., 2021), turbidite-dominated mixed systems (Gong et al., 2013, 2016) or hybrid systems (Sansom, 2018; Fuhrmann et al., 2020). The nature of each of these systems varies due to the level of interaction, current velocity, density and frequency of turbidity currents versus bottom currents (Haughton et al., 2009; Mutti et al., 2014; García et al., 2015).

Recent studies have identified distinct morphological elements at a low- to medium-resolution spatial scale (>100 m – 1 km; Gong et al.,

2013, 2020; Fonnesu et al., 2020; Batchelor et al., 2021; Pandolpho et al., 2021). Most of these studies are based on multichannel seismic data, which span long temporal scales and do not provide sufficient spatial coverage and vertical resolution to understand the variability of mixed systems in detail. Furthermore, several authors recognize a significant lack of studies with a high spatial and vertical resolution (10–100 m) across modern deep-water environments (Rebesco et al., 2002; Gong et al., 2013; Levin et al., 2019) and in ancient systems (Shanmugam et al., 1993; Viana et al., 1998; Fonnesu et al., 2020). As such, high-resolution studies are needed to better understand mixed systems and their deposits in more detail. An analysis of modern mixed systems and comparison with their ancient counterparts is further encouraged to establish the link between the different processes and products at a high-resolution scale and to address the various models and their uncertainties.

The Pacific margin of the Antarctic Peninsula (PMAP) hosts one of the most extensive, modern mixed depositional systems (Fig. 1A), characterized by distinct erosional and depositional features (Rebesco et al., 1998, 2002; Amblas et al., 2006; Hernández-Molina et al., 2017), which collectively account for the depositional style of the margin (Hernández-Molina et al., 2006, 2017; Rebesco et al., 2007; Amblas and Canals, 2016). It is also one of the best studied examples, with extensive swath bathymetry coverage, 2D multichannel seismic reflection lines, a dense network of acoustic sub-bottom profiles and numerous shallow sediment cores and deep drill cores, making it a suitable candidate to build upon previous knowledge and to better understand the vertical and lateral variability of mixed systems at a high-resolution spatial scale. As such, the PMAP offers an exceptional site to investigate the interaction between along- and down-slope processes and their associated elements. Thus, the objectives of this work are: i) to identify key depositional and erosional features along the modern mixed depositional systems, ii) to characterize their sedimentary stacking patterns and evolution during the Quaternary, and iii) to propose a sedimentary model, which can be compared to other mixed systems in modern oceans or in the ancient record.

2. Geologic and physiographic settings

2.1. Geological history

The PMAP (Fig. 1) corresponds to a passive continental margin at present, which used to be active between the Early Cretaceous and late Neogene (Larter et al., 1997; Jin et al., 2002; Poblete et al., 2011; Nerlich et al., 2013). The progressive migration of the Antarctic-Phoenix spreading ridge towards the former trench that ran along the PMAP eventually led to ridge-crest trench collisions. As the ridge segments arrived at the trench, from SW to NE, subduction locally ceased and trench topography was eliminated. The area SW of the PMAP became passive in the middle Eocene, and the transition from active to passive then migrated progressively NE-ward along the margin (Larter and Barker, 1989, 1991b; Larter et al., 1997). After an initial phase of uplift for each collision segment (that lasted between 1 and 4 Myr), subsidence began to occur as a result of thermal decay, sediment deposition and compaction that still continues today (Larter and Barker, 1989, 1991a; Larter et al., 1997; Yegorova and Bakhmutov, 2013; Hernández-Molina et al., 2017). At present, slow convergence continues north of the Hero Fracture Zone (HFZ) (Fig. 1), at the South Shetland Trench.

The continental shelf and slope along the southern part of the PMAP contain a thick sedimentary succession (Larter and Barker, 1989; Larter and Cunningham, 1993; Larter et al., 1997) for which three main phases of evolution have been proposed (Hernández-Molina et al., 2017): 1) Early Cretaceous to middle Miocene non-glacial transition from active to passive margin; 2) glacially-influenced middle to late Miocene aggradational sedimentary stacking and subsidence; and 3) fully-glaciated late Miocene to early Pliocene formation of progradational to aggradational units.

The continental rise hosts a thick succession of clastic sediments that comprise the large mixed depositional systems, characterized by huge sediment drifts and vast trunk channels (Fig. 1A) (McGinnis and Hayes, 1995; McGinnis et al., 1997; Uenzelmann-Neben, 2006; Lucchi and Rebesco, 2007). Previous studies have provided the seismic and lithostratigraphic framework for the formation and long-term evolution of these mixed systems (Rebesco et al., 1996, 1998, 2002; Dowdeswell et al., 2004; Amblas et al., 2006; Hernández-Molina et al., 2017). The main features first started to develop in the Miocene (15 Ma ago) after a preceding *pre-drift stage* (from 36 to 15 Ma) dominated by turbiditic systems. The drifts have two distinct stages of evolution, *drift-growth* (15–5 Ma) and *drift-maintenance* (5–0 Ma) (Rebesco et al., 1997, 1998, 2002; Uenzelmann-Neben, 2006). Our study focuses on the latest phases of the *drift-maintenance* stage at a high-resolution spatial scale, for a better understanding of deep-water sedimentary process interactions and to decode the short-term evolution of these mixed depositional systems.

2.2. Physiographic domains

The PMAP comprises three main regional physiographic domains: the continental shelf, slope and rise (Fig. 2). The continental shelf trends NE-SW with a gentle landward 0–1° dip (see Fig. S1 in the *supplementary material*) and reaches 500 m water depth on average at the shelf break (Fig. 2). The shelf extends over a length of 2000 km in the studied area and up to 350 km in width. This domain has two prominent features: banks (or highs) and troughs (Fig. 2; Rebesco et al., 1998; Lavoie et al., 2015). Four major banks occur along the outer shelf of the central part of the PMAP at 350–400 m water depth as 200 m high, positive reliefs above the surrounding seafloor. The banks are separated by 5–6 troughs and smaller erosive features, of which the Marguerite Trough is the most prominent (Livingstone et al., 2013). The troughs often form U-shaped, elongated depressions, mainly trending from WNW-ESE to N-S (Fig. 2). The troughs also include glacial geomorphological features, such as mega-scale glacial lineations (Fig. 2) and iceberg plough marks in the middle and outer shelf trough sections, whereas meltwater channels, drumlins and scoured bedrock occur in the inner shelf sections (e.g., Canals et al., 2000; Ó Cofaigh et al., 2002; Heroy and Anderson, 2005; Livingstone et al., 2013; Larter et al., 2019).

The continental slope stretches from 500 m down to ca. 3000 m water depth (Fig. 2). The upper and middle slope can be considered steep (with slope angles around 10–13° and 16°, respectively), while the lower slope is relatively gentle (~2–5°) (Fig. S1; cf. Dowdeswell et al., 2004). The upper continental slope is heavily incised by numerous NW-SE subparallel gullies, some of them 100 m wide and 100 m deep (Fig. 2; Dowdeswell et al., 2004; Heroy and Anderson, 2005; Gales et al., 2013).

The continental rise extends from ca. 3000 to 4500 m water depth (Tucholke and Houtz, 1976; Tucholke, 1977) and holds the modern mixed depositional systems along the upper continental rise (Fig. 1A; Rebesco et al., 1996, 1998, 2002; Larter et al., 1997; Hernández-Molina et al., 2017). They comprise massive, complex mounded drifts and trunk channels, fed by a dendritic network of channels and gullies spread across the lower continental slope and upper continental rise (Figs. 1A and 3). These features trend perpendicular to the margin and cover 990,000 km^2 (Fig. 2). In addition, the Tula, Biscoe, Hero and other fracture zones run across the continental rise, which are mostly buried beneath a thick sediment cover on the upper to middle rise (Figs. 1A and 2).

3. Oceanographic setting

Oceanic circulation along the PMAP involves dynamic interactions between the water masses of the Southern Ocean (Fig. 1A). The eastward flowing Antarctic Circumpolar Current (ACC) is the world's largest ocean current; it flows around the Antarctic continent, driven by westerly winds (Fig. 1A), with an average net baroclinic transport of 173
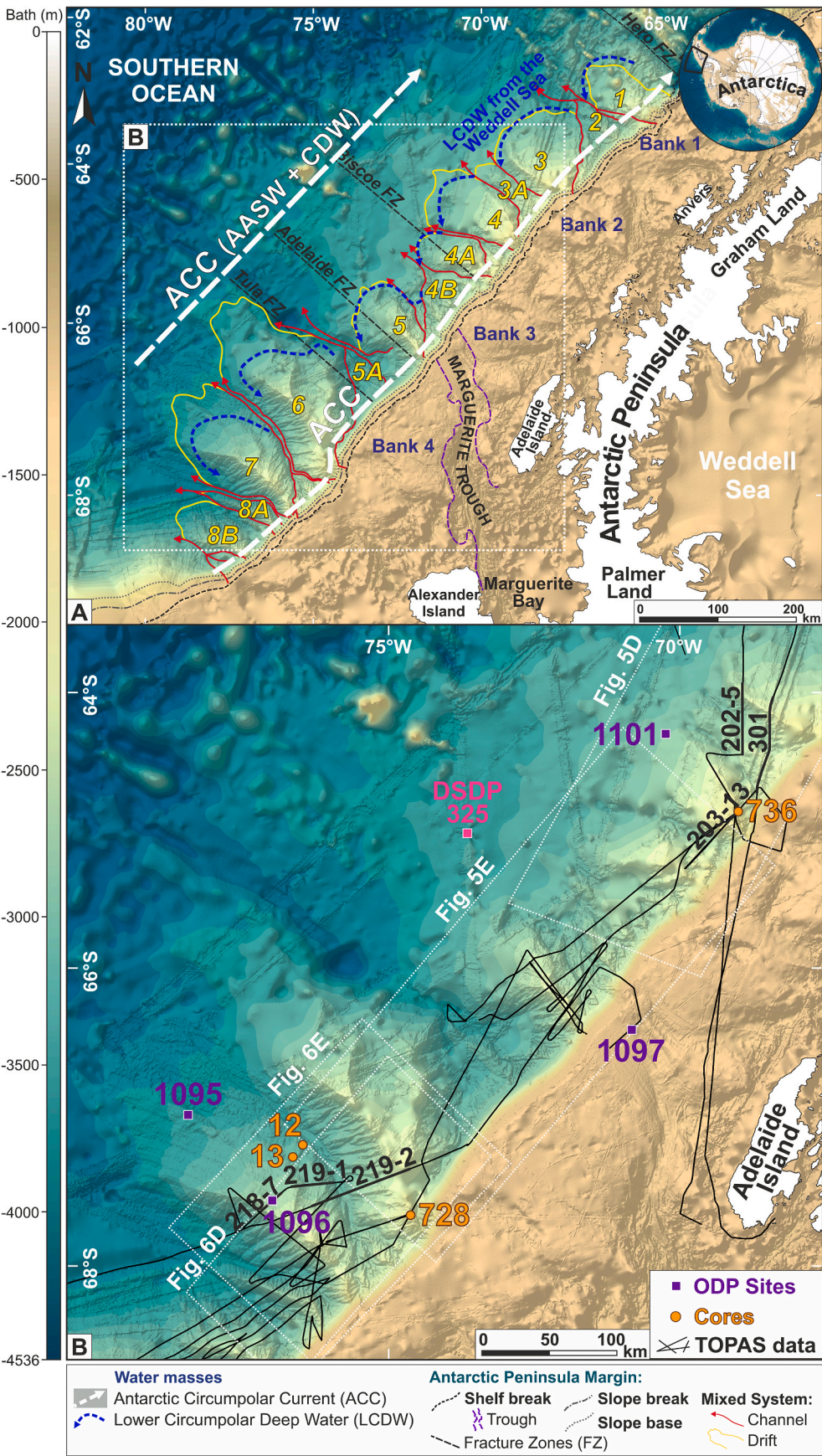
Fig. 1. A) Location of the modern mixed (turbidite-contourite) systems and main water masses circulating around the PMAP; and B) location of TOPAS acoustic sub-bottom profiles used in this study, as well as sediment cores, ODP, and DSDP drill sites. Oceanic circulation after Orsi et al. (1995, 1999), Camerlenghi et al. (1997), Giorgetti et al. (2003) and Palmer et al. (2012). Multibeam bathymetry from GEBCO (2019). AASW – Antarctic Surface Water; ACC – Antarctic Circumpolar Current; CDW – Circumpolar Deep Water; LCDW – Lower Circumpolar Deep Water.
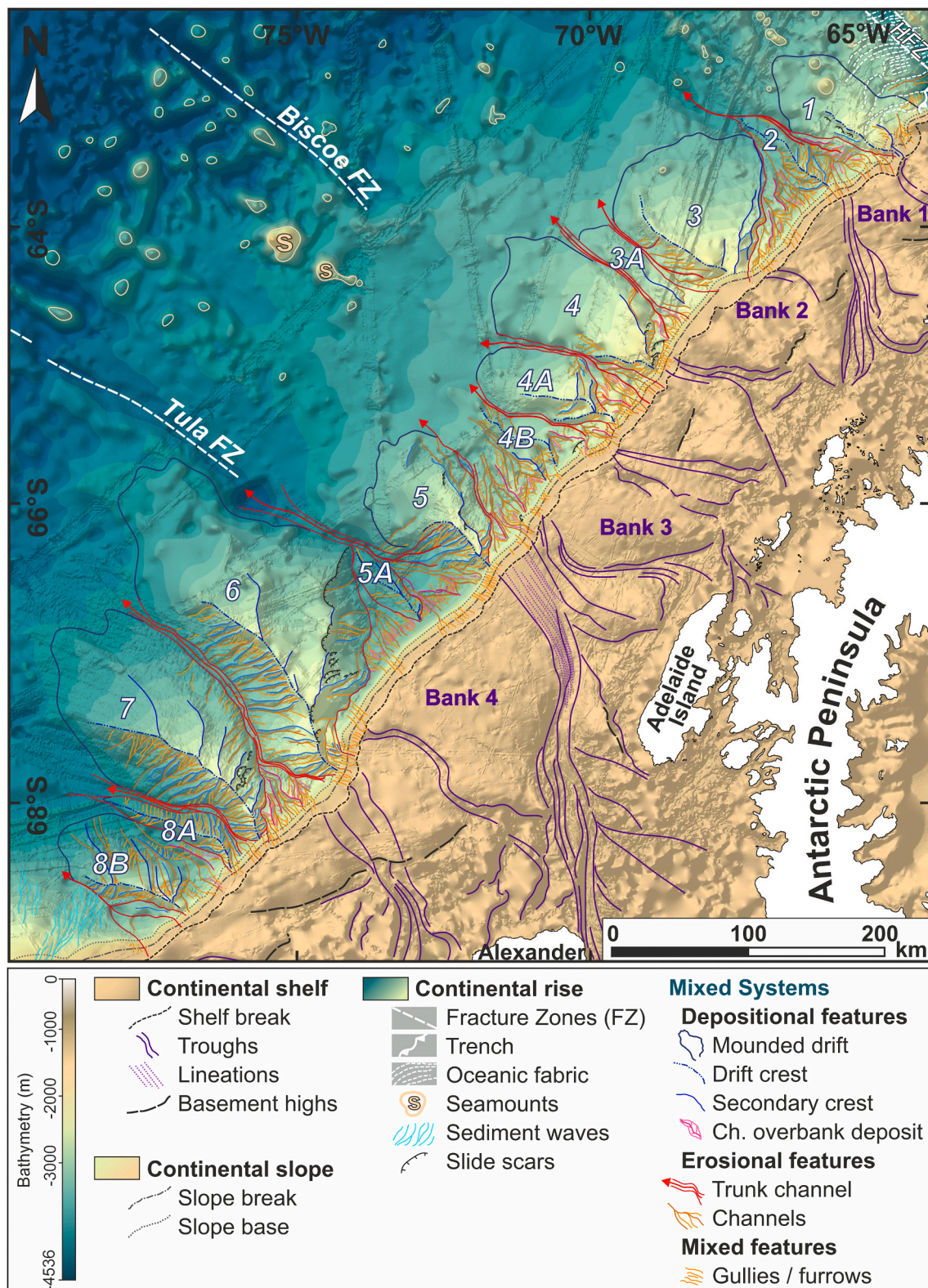
Fig. 2. Morphological map showing the main physiographic domains highlighting the main morphological features of the modern mixed depositional system. HFZ – Hero Fracture Zone.

Sverdrup (Sv) (1 Sv equals 10^6 m^3 s^{-1}) through the Drake Passage (Donohue et al., 2016). The ACC comprises several bottom-reaching fronts, which dip preferentially northward (Naveira Garabato et al., 2002, 2003).

On the PMAP, the main water masses are Antarctic Surface Water

(AASW) and Circumpolar Deep Water (CDW) (Fig. 1A). The relatively fresh AASW flows between the sea surface and 200 m water depth with a temperature $< 0\,°C$ and salinity typically >34.0 psu (Carter et al., 2009). AASW comprises the very cold Winter Water (WW) below the surface mixed layer, identified by a temperature minimum of $<-1\,°C$ (Nowlin
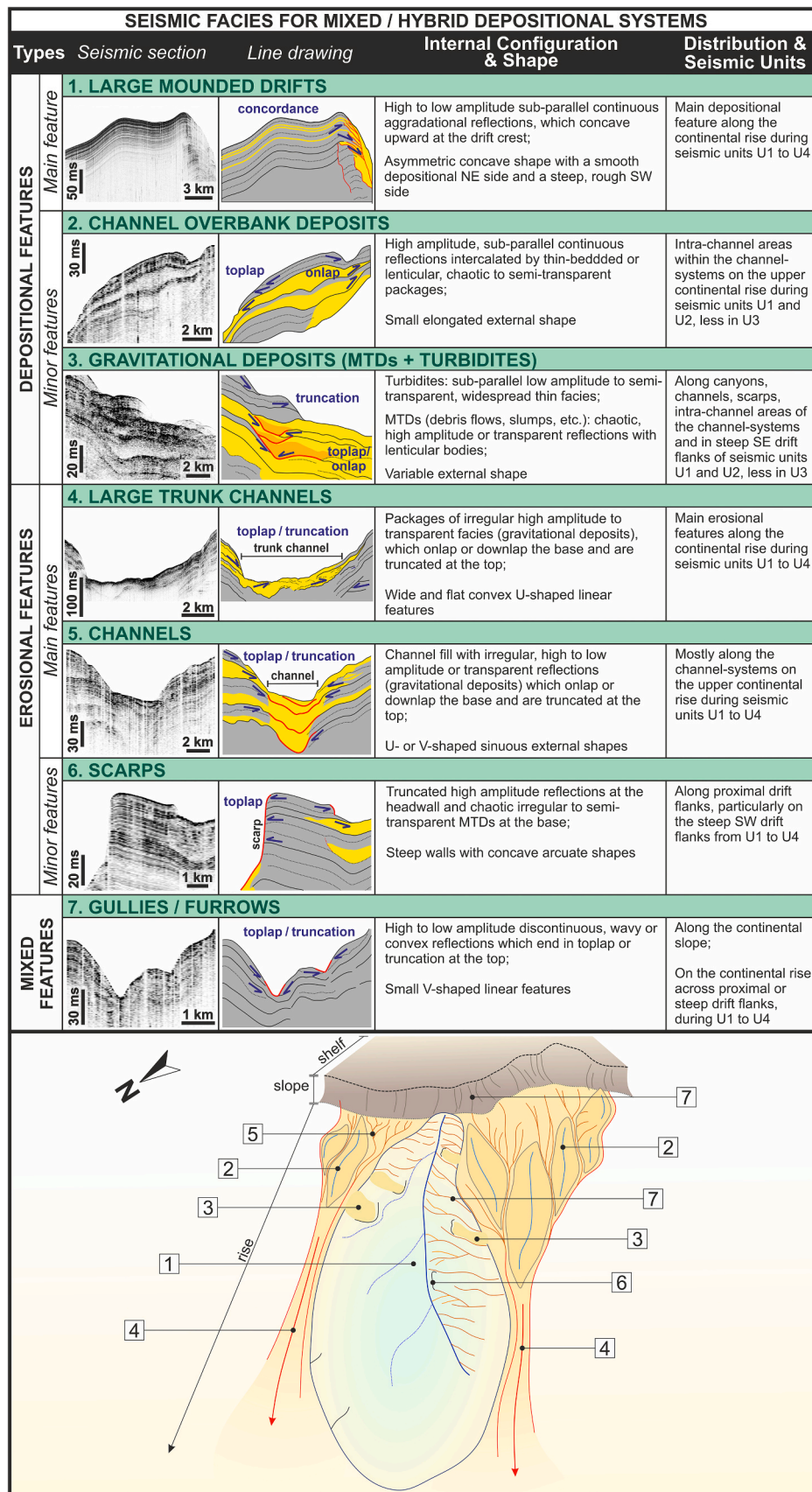
Fig. 3. Acoustic facies for mixed depositional systems. Based on acoustic sub-bottom profiles of TOPAS. Blue arrows represent reflection terminations; red lines represent erosional surfaces. (For interpretation of the references to colour in this figure legend, the reader is referred to the web version of this article.)

Jr. and Zenk, 1988). The surface mixed layer corresponds to a 100 m thick layer warmed and freshened by ice melting during summer periods (Patterson and Whitworth, 1989) and is identified by a salinity <34.40 psu and a potential temperature < 0.5 °C (Giorgetti et al., 2003).

CDW is characterized by a relatively high salinity >34.6 psu and high temperature > 0–2 °C (Dinniman et al., 2011), flowing primarily towards the NE at 200–3000 m water depth within the ACC (Fig. 1A). CDW is divided into Upper Circumpolar Deep Water (UCDW), originating primarily from the Southeast Pacific Ocean and Western Indian Ocean, and Lower Circumpolar Deep Water (LCDW), a remnant of the more saline North Atlantic Deep Water (NADW) input into the ACC (Hillenbrand et al., 2008; Fig. 1A). The core of the UCDW is centred at ca. 1000 m water depth, marked by an oxygen minimum and a maximum in nutrients and temperature (Ito et al., 2010). In the study area, LCDW also flows primarily towards the NE within the ACC, but a branch originating from the Weddell Sea flows SW-ward along the continental rise at roughly 3500 m water depth (Fig. 1A). This branch has a mean current velocity of ~6 cm s^{-1}, maximum speed of 20 cm s^{-1}, potential temperature of 0.11–0.13 °C, and salinity up to 34.70 psu (Camerlenghi et al., 1997; Giorgetti et al., 2003). The sediment drifts and channel systems in the upper part of the continental rise appear to be influenced by this branch of modified LCDW (Fig. 1A).

4. Data and methods

Bathymetric data and acoustic sub-bottom profiles were used to study the mixed depositional systems along the PMAP at 10–100 m spatial and vertical scale (Figs. 1B, 4 and 5).

4.1. Datasets

4.1.1. Bathymetry

The bathymetric data for the maps presented in this study consists of the global GEBCO, 2019 dataset (GEBCO, 2019), which is a compilation of the available multibeam and single beam data produced by the International Bathymetric Chart of the Southern Ocean (IBCSO) across the Antarctic continental margin (Arndt et al., 2013). The dataset was interpolated to 100 m cell size and projected with the Antarctic Polar Stereographic Projection to minimize distortion. The dataset covers the entire PMAP, from the shelf to about 4500 m water depth on the continental rise (Fig. 1B).

4.1.2. Sub-bottom profiles

This study uses high-resolution Topographic Parametric Sonar (TOPAS) data provided by the British Antarctic Survey (BAS) (Larter et al., 2021). The TOPAS profiles were acquired during cruise JR298 with RRS *James Clark Ross* in 2015. This dataset was logged using a Kongsberg Simrad TOPAS PS018 sub-bottom profiler. The TOPAS system operated by transmitting a chirp pulse with a frequency band of 1.5–5 kHz and length of 10 ms. The receiver had a sample rate of 20 kHz with a trace length of 400 ms, and the gain (in dB) was controlled by the sonar watch with a range of 2–15 dB and a HP-filter of 1–2 kHz. The return signals were cross-correlated with the source signature (matched filter) throughout the cruise to extract signals with a simple effective waveform, which also has the benefit of reducing random noise. The data was processed onboard and at BAS before being made available for this study.

4.2. Chronological constraints from core data

During Ocean Drilling Program (ODP) Leg 178 in 1998, nine sites were drilled across the PMAP to investigate Antarctic glacial history and sea-level change (Barker et al., 1999, 2002). Our work uses published biostratigraphic and magnetostratigraphic data from Site 1096, drilled on the crest of Drift 7 (Fig. 1B), to provide chronological constraints for the TOPAS data (Barker et al., 1999, 2002). During ODP Leg 178, a

nearly continuous magnetostratigraphic record was obtained for Site 1096 from polarity changes detected in the inclination data of the sediment cores (Acton et al., 2002). Biostratigraphic constraints were obtained from first and last appearance datums mainly of diatoms, with a few age constraints provided by radiolarians and calcareous nanno-fossils (Iwai et al., 2002). Calcareous microfossils occurred only in relatively short core intervals that alternated with barren intervals (Barker et al., 1999). A combination of the available biostratigraphic and paleomagnetic data established an age model for Site 1096 (Fig. 6E; Barker et al., 1999; Iwai et al., 2002), which was used to estimate the ages of the uppermost sediments imaged in the TOPAS data (see "*Stratigraphic correlation between core and seismic data*" in Subsection 4.3 of the Methodology section for details). Sedimentary records of Site 1096 as well as Sites 1095 and 1101 drilled on the distal flank of Drift 7 and the crest of Drift 4, respectively (Fig. 1B), were used to provide lithological information for the studied stratigraphic interval (Fig. 6F; Barker et al., 1999).

Furthermore, previously published high-resolution age models for piston cores PC736 and PC728 (Fig. 1B) collected during cruise JR298 in 2015 (Channell et al., 2019) and gravity cores SED-12 and SED-13 (Fig. 1B) recovered by the PNRA (Italian national program of research in Antarctica) SEDANO-II Project in 1998 (Lucchi et al., 2002) were used as age constraints for the sediments in the uppermost ca. 10 m of the seabed. These age models are based on relative paleointensity (RPI) studies published by Sagnotti et al. (2001), Macrì et al. (2006), Venuti et al. (2011), Vautravers et al. (2013) and Channell et al. (2019). The RPI dating method measures past variations in the Earth's magnetic field intensity archived in the marine sediments. The down-core RPI results from PMAP cores, such as PC728 and PC736, were directly correlated with RPI reference curves compiled from stacked RPI records of marine sediment cores recovered from various ocean basins around the globe, which had been independently dated, mainly by orbitally tuned fora-minifera δ^{18}O stratigraphy (Sagnotti et al., 2001; Macrì et al., 2006; Channell et al., 2019). The RPI records of cores SED-12 and SED-13 were dated by Venuti et al. (2011) by correlating their magnetic parameters with those of nearby SEDANO cores previously RPI-dated by Sagnotti et al. (2001). All these studies provided high quality age models supported by correlations with neighbouring cores, for which biostratigraphic datums from diatoms and nannofossils (Pudsey and Camerlenghi, 1998; Pudsey, 2000, 2002; Lucchi et al., 2002; Villa et al., 2003) or tephrochronological age constraints (Hillenbrand et al., 2021) were available, and which showed systematic down-core changes in productivity proxies (e.g., Ba/Al and Br/Al ratios) and in sediment li-thology and provenance (e.g., clay mineralogy) that reflect cyclic variations in biological productivity and terrigenous supply on glacial-interglacial timescales (Pudsey and Camerlenghi, 1998; Pudsey, 2000; Lucchi and Rebesco, 2007; Channell et al., 2019; Hillenbrand et al., 2021).

4.3. Methodology

4.3.1. Seismic processing

The combination of bathymetry and sub-bottom profiles allowed us to identify the main morphological features in the mixed systems. The TOPAS sub-bottom profiles were used to characterize the upper sedi-mentary sequence (down to ≤150 ms two-way travel time [TWT], cor-responding to ~115 m below seafloor) of the mixed systems in terms of their acoustic response, seismic facies and reflection configuration pat-terns. Loss of signal amplitude with increasing depth below the seafloor is typical for very high-resolution sub-bottom profiles because higher frequencies are more strongly affected by attenuation. Reflections are clearly imaged down to 100 ms TWT below the seafloor with a vertical resolution of <1 m. Post-processing included bandpass filtering, bottom tracking, time variable gain and automatic gain control. The TOPAS profiles were visualized in IHS Kingdom Suite Software via the seismic attribute 'Envelope' and a bandpass filter with the following frequency
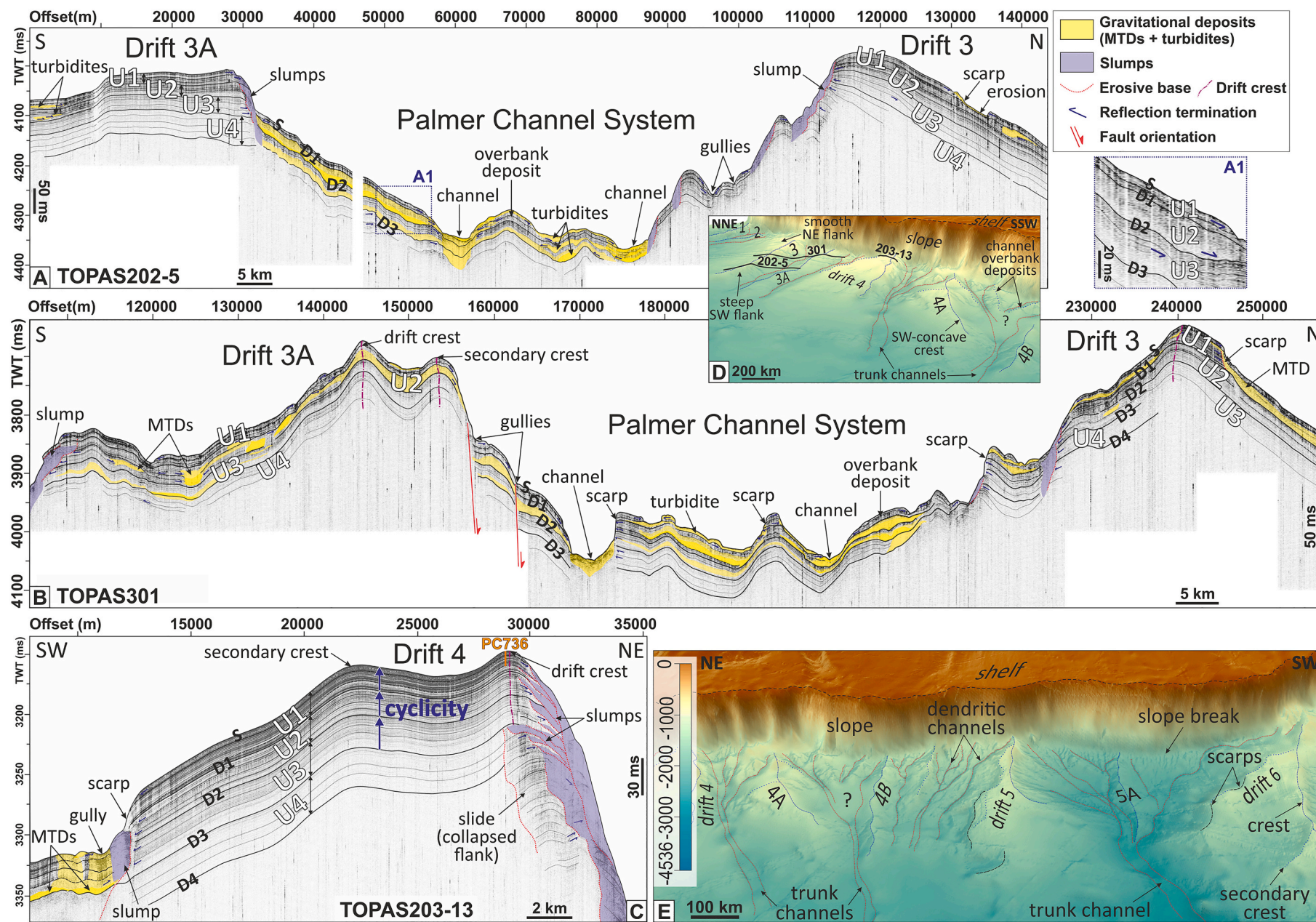
Fig. 4. TOPAS acoustic sub-bottom profiles 202–5 (A), 301 (B) and 203–13 (C) showing the main acoustic units (U1 to U4), discontinuities (D1 to D4) and morphological features of Drifts 3 to 6 (D, E) of the mixed depositional systems. S: seafloor. Location of TOPAS lines and maps in Fig. 1B. Uninterpreted versions included in the *supplementary material*.

Fig. 5. TOPAS acoustic sub-bottom profiles 219–2 (A), 218–7 (B) and 219–1 (C) showing the main acoustic units (U4 to U1), discontinuities (D4 to D1) and morphological features of Drifts 6 and 7 (D, E) of the mixed depositional systems. S: seafloor. Location of TOPAS lines and maps in Fig. 1B. Uninterpreted versions included in the *supplementary material*.
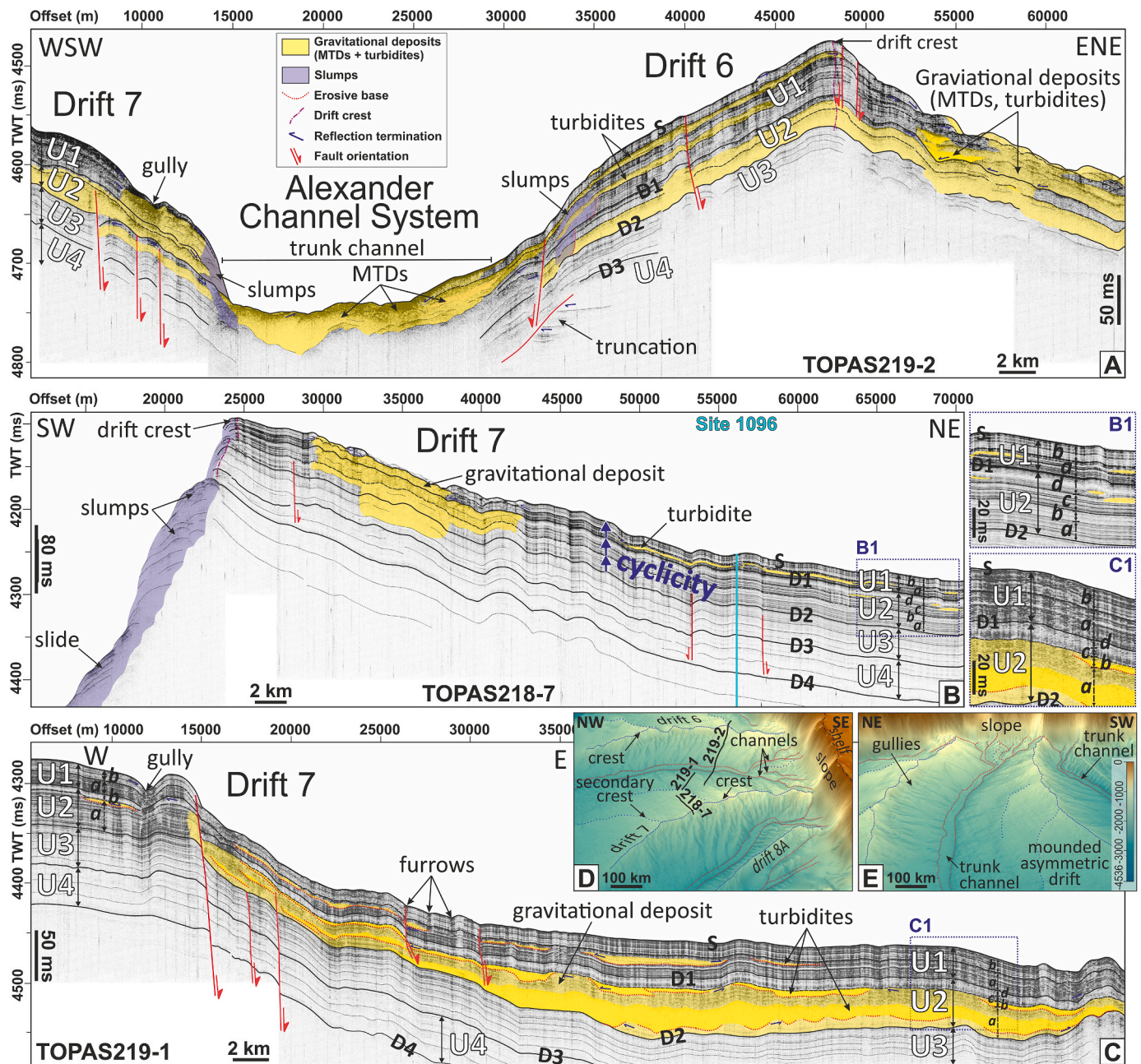
values: low cut: 1200 Hz; high pass: 1700 Hz; low pass: 4800 Hz; high cut: 5200 Hz. Un-interpreted versions of the sub-bottom profiles shown in this study are given in the *supplementary material* (Figs. S2 and S3).

4.3.2. Stratigraphic correlation between seismic and core data

The stratigraphic correlation between the seismic and core data used the time-to-depth conversion and velocity model established during ODP Leg 178 for Site 1096 (Barker et al., 1999; Volpi et al., 2001). *P*-wave velocities were measured with a Hamilton Frame (PWS3) and used to produce time-to-depth curves (shown in Fig. S4C of the *supplementary material*). The time-to-depth relationships were compared with the Carlson et al. (1986) standard time-to depth relationship and with the polynomial regression established for the vertical seismic profile data at Site 1095 (Barker et al., 1999; Volpi et al., 2001). As there was a substantial similarity between all three datasets (see Fig. F57 in Site 1096

chapter of Barker et al., 1999), a time-to-depth relationship was established through linear interpolation (Fig. S4C) and used to generate a synthetic seismogram with the assistance of density and velocity data acquired at Site 1096 (Volpi et al., 2011). The synthetic traces were adjusted and equalized to the seismic traces of multichannel seismic profile IT95–130 (Fig. 6B). This final step produced four main tie points (see checkshot data in Table T35 of Barker et al., 1999) and along with the time-to-depth relationships allowed the integration of Site 1096 lithostratigraphic and seismostratigraphic units across multichannel seismic profile IT95–130 (Fig. 6B and 6F). The checkshot data, along with the previously established velocity model (Fig. S4C), were used to tie Site 1096 to seismic profile TOPAS 218–7 (Fig. 6C). Using the four main tie points and the linear interpolation of the time-to-depth conversion (Fig. S4C), we plotted the lithologies and ages of Site 1096 on top of the TOPAS data (Fig. 6C), thus obtaining chronological
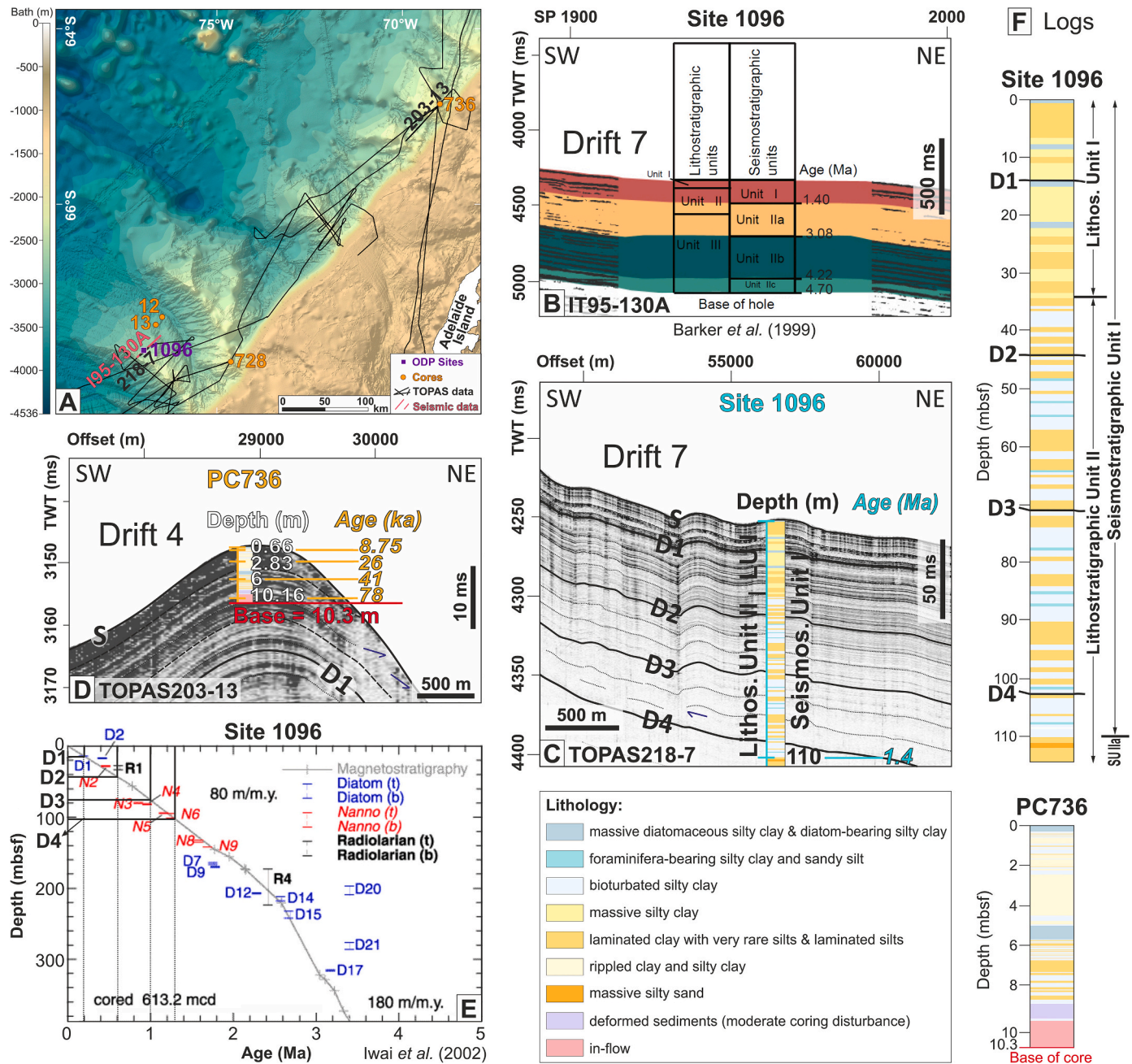
Fig. 6. Correlation between the seismic discontinuities D1-D4 and the chronostratigraphic ages, lithostratigraphic and seismostratigraphic units of ODP Leg 178 Site 1096, from Barker et al. (1999) and Iwai et al. (2002), and of PC736 after Channell et al. (2019). A) Location of TOPAS acoustic sub-bottom profiles and sediment core data used for the chronological constraints; B) multichannel seismic reflection profile IT95–130A shown in Barker et al. (1999) with the seismostratigraphic and lithostratigraphic units of Site 1096; C) correlation between sub-bottom profile TOPAS 218–7 and Site 1096; D) correlation between sub-bottom profile TOPAS 203–13 and sediment core PC736; E) chronostratigraphic ages and sedimentation rates shown in Iwai et al. (2002), overlain by the seismic discontinuities D1-D4 identified in this study; and F) summarized logs for Site 1096 and core PC736.

constraints for the imaged sediments (Fig. 6C and 6E).

P-wave velocities were measured with a multi-sensor core logger (MSCL) across core PC736 (Hillenbrand et al., 2021). These measurements were used to produce a time-to-depth curve (shown in Fig. S4) and generate a synthetic seismogram. The synthetic traces were equalized to the acoustic traces of profile TOPAS 203–13, which allowed us to tie core PC736 to the TOPAS data (Fig. S4). This step, along with the estimated time-to-depth model, allowed the correlation of the chronological ages and lithologies of PC736 with profile TOPAS 203–13 (Fig. 6C and 6E).

4.3.3. Seismic stratigraphy

Seismic stratigraphic analysis followed the conceptual methods established by Mitchum et al. (1977) and Catuneanu et al. (2009). Different elements formed in high-latitude settings due to the presence of ice, with respect to their lower latitude counterparts, are discussed by Zecchin et al. (2015). Based on their approach, we were able to identify significant continuous or erosional surfaces, distinct stacking patterns and different morphological features. For the uppermost sediments and at the seafloor, we differentiate large- and small-scale features based on their: 1) orientation, 2) external geometry, 3) dimensions, 4) bounding surfaces, and 5) internal configuration (Fig. 3). Their designation as

depositional or erosional features follows the criteria proposed by Faugères et al. (1999), Rebesco et al. (2014), Fonnesu et al. (2020) and Rodrigues et al. (2021). Their studies define gullies, channels, levees, gravitational deposits (turbidites and mass-transport deposits = MTDs) and sedimentary lobes as erosional or depositional features generated by down-slope processes, while along-slope features, such as contourite drifts, terraces, moats and contouritic channels, were formed or substantially reworked by the persistent action of bottom currents.

5. Results

5.1. Seismic stratigraphic analysis

Four major seismic units (U1-U4), separated by four main discontinuities (D1-D4), were identified below the present seafloor (S) in the TOPAS profiles (Figs. 4 and 5). Seismic facies exhibit low to high amplitude, continuous and parallel reflections, whose amplitude increases towards the top for U1-U3 (Fig. 5A1), with relatively high continuity across the mounded drifts and less continuity across the complex channel systems (Fig. 4B). The identified seismic units are locally absent near the trunk channels. This absence most likely results from erosion as thin beds of acoustically transparent bodies or lenses corresponding to turbidites and MTDs are observed in the vicinity of the channels (Fig. 5A). Seismic units U1-U4 have an average thickness of 25–40 ms TWT (Fig. 4C), which increases up to ~50–60 ms TWT along drift crests (Fig. 5B) and decreases down to <25 ms TWT near trunk channels and across the distal drift flanks facing the deep sea (Fig. 4E). The units display lenticular to sheeted morphologies and are separated by discontinuities D1-D4 that are mostly conformable over the mounded drifts (Fig. 5B) and become unconformable near trunk channels (Fig. 5A) and along the proximal flanks close to the continental slope. Detailed descriptions for each unit are given in Table 1.

5.2. Morphological elements of the modern mixed systems

Seven distinct morphological features were identified in the bathymetric data and TOPAS sub-bottom profiles (Fig. 3). Based on their external shapes and internal configurations, these have been interpreted as: 1) large, mounded drifts, 2) channel overbank deposits, 3) gravitational deposits, 4) large trunk channels, 5) channels, 6) scarps, and 7) gullies/furrows. A total of 13 large contourite drifts occur from 2700 to 3900 m water depth, separated by 12 extensive turbidite channel systems developing between 2500 and 4000 m water depth (Fig. 2).

5.2.1. Depositional features

5.2.1.1. Large elongated mounded drifts.
Thirteen mounded drifts, elongated sub-perpendicularly to the margin trend, form the main depositional features between 2700 and 3900 m water depth (Fig. 2). The drifts exhibit asymmetric SW-concave morphologies, except Drift 3, which concaves towards NE (Fig. 2). Their shape is usually formed by a smooth NE depositional flank and a rugged, steep SW flank; exceptions are Drift 5, where both flanks are heavily eroded, and Drift 8A, which has a relatively smooth SW flank and a rough NE flank (Fig. 2). On the upper continental rise, the drifts are characterized by a steep (2–10°) proximal flank that runs oblique or parallel to the margin (Fig. S1), whereas their distal flanks facing the deep sea are smooth and gentle (0–2°) (Fig. 2). The proximal flanks are usually incised by sub-parallel NW-SE oriented gullies, perpendicular to the margin (Figs. 2 and 3). The largest drifts rise up to 1 km above the surrounding seafloor and are 70–100 km wide and 150–250 km long (Fig. 2). Seismic units U1-U4 present 25–40 ms TWT average thicknesses over the NE flanks (Fig. 5B), which increase slightly up to ~50 ms TWT at the drift crests (Fig. 5C) and decrease until >25 ms TWT along the SW flanks (Fig. 4A). Sedimentary thicknesses also increase from the proximal flanks, around ca. ~25–40 ms TWT (and up to 60–70 ms TWT) and decrease to <30 ms TWT further seaward due to their lenticular shape. Discontinuities D1-

Table 1

Seismic characteristics of the main seismic units (U1 – U4) and their discontinuities (D1 – D4). The discontinuity described in each seismic unit corresponds to the basal boundary. TWT: two-way-travel time; MTDs: Mass transport deposits.

Seismic Units	Seismic Discontinuities	Internal Reflection Configuration		Reflection terminations	Unit shape	Thickness (TWT)
U1	D1	Laterally continuous, sub-parallel, high amplitude reflection, conformable with the underlying U1	Continuous, sub-parallel, high to low amplitude reflections with well-stratified aggradational facies. U1 is divided in sub-units U1a and U1b due to repeated loss of amplitude signal towards the top. Smaller seismic facies variations define internal sequences U1a$_1$ to U1b$_2$	Reflections toplap or end in truncation near and within channels, or against MTDs	Widespread, uniform sheet, locally interrupted by thin MTDs and turbidites across channels, steep drift flanks and gentle depressions in the depositional flanks	25–40 ms, up to 55 ms
U2	D2	Laterally continuous, sub-parallel, high amplitude reflection, conformable with the underlying U3	Continuous, sub-horizontal, high to low downlap reflections along the top of NE drift flanks, transition laterally into chaotic, irregular, semi-transparent to high amplitude reflections along drift flanks and within channels. U2 is divided in seismic sub-units U2a and U2b by changes in its seismic facies, and further sub-divided as internal sequences U2a$_1$ to U2b$_2$	Reflections onlap or downlap against D2 and end in toplap or local truncations against D1	Uniform aggradational sheet along the drifts changes laterally towards channel-fill facies across the channels, interrupted by lenticular MTDs or thin-bedded turbidites	30–40 ms along the drifts and ~50 ms thick in the channels
U3	D3	Laterally continuous, conformable, high amplitude reflection	Laterally continuous, sub-parallel, low to high amplitude reflections, with stratified facies and increasing amplitude signal towards the top	Conformable with D3 and D2; localized onlap near channel margins and in proximal drift flanks	Uniform, aggradational sheet	30–40 ms, up to 60 ms
U4	D4	Prominent, laterally continuous, conformable, high amplitude reflection	Sub-parallel, laterally continuous low amplitude reflections with stratified facies	Conformable with D4 and D3, with small, local truncations against D3	Thick aggradational sheet draped over previous mounded morphologies	40–50 ms, up to 70 ms

D4 are mostly conformable across the mounded drifts but end in toplap or truncations near channel margins and local MTDs or turbidites (Figs. 4B and 5A).

On most of the drifts, the steep (2–6°) and rough SW flanks are marked by widespread gravitational scars and often parallel gullies, in general oriented perpendicular to the drift's crests in a N*E*-SW direction and, thus, perpendicular to the channel system trend (Fig. 2). Overall, these gullies are <100 m deep and 1–3 km wide (Fig. 4B). The SW flanks are characterized by extensive MTDs, such as slides and slumps (Fig. 5B), with NE-SW oriented crests, preserved in between gullies (Fig. 5A). The MTDs have high amplitude to semi-transparent reflections with variable configurations and thicknesses (Fig. 5A). Across the SW flanks, U1-U4 thicknesses are ~25 ms TWT, but they can reach >30 ms TWT in between gullies (Fig. 4B) and close to the drift crests (Fig. 5A). Their discontinuities D1-D4 are conformable near drift crests but often end in toplap near the complex channel systems (Fig. 5A).

The NE flanks of most drifts are smooth and have gentle slopes (0–2°) with aggradational sediments (Fig. 5B). The NE flanks exhibit arcuate slide scarps and NW-SE to E-W oriented gullies at their base or close to the main trunk channel further NE (Fig. 2). These scarps and gullies may be related to normal faults, especially near the complex channel systems and their trunk channels (Figs. 4B and 5A). The internal configuration of the NE flanks is characterized by high to low amplitude, continuous aggradational deposits some 50–100 ms TWT thick (Fig. 5B), intercalated with irregular, chaotic, high amplitude to semi-transparent lenticular MTDs or thin-bedded turbidites with thicknesses of approximately 20–50 ms TWT (Fig. 5C). Seismic units U1 to U4 present average thicknesses of 25–40 ms TWT (which can reach up to 60–70 ms TWT) along the gentle slopes of the NE flanks (Fig. 5B), which decrease below <25 ms TWT near the trunk channels (Fig. 5A). Discontinuities D1-D4 are mostly conformable across the NE drift flanks (Fig. 5B), but end in toplap or truncation against local MTDs, scarps and near the channel margins (Fig. 5A).

The drifts have narrow, curved NW-SE striking crests located at 2500–2900 m water depths (Fig. 2). These crests display a wide concavity towards the steeper SW flanks and their apexes point towards the gentle NE flanks (Fig. 2). Drift 3 is an exception, as its crest concaves towards the NE flank (Fig. 2). Drift crests have several inflections, caused by the local development of arcuate erosional scars and gullies on the SW flanks, and on the NE flank of Drift 5, respectively (Fig. 2). Secondary drift crests branch northward from the main drift crests at oblique angles (~30°) (Fig. 2). The secondary crests separate gentle slopes within the NE flanks in step-like patterns. Sediments are locally thicker at the base of these slopes (up to 150 ms TWT in U1-U4), due to the presence of downward thickening, high amplitude to semi-transparent reflections intercalated with high amplitude, continuous, in general parallel reflections (Fig. 5C).

5.2.1.2. Channel overbank deposits.

Small, elongated, channel overbank deposits (Fig. 3) occur within the dendritic channel-complex systems along the upper continental rise. The channel deposits start at variable water depths, between 2800 and 3300 m and reach down to 3300–3900 m (Fig. 2). These features trend NW-SE or NNW-SSE, parallel to the channel system trend (Fig. 3). The channel overbank deposits exhibit asymmetric to symmetric bar shapes, which start as a sharp diverging triangle before elongating down-slope and ending again in a triangular shape (Fig. 3). They are 100–300 m high, 20–70 km long and ~ 20 km wide (Fig. 4A and 4B). Their surface is intensely scoured by small 100 m deep sub-parallel gullies trending *E*-W on the SW flanks and N-S on the NE flanks. These gullies are oriented oblique and point towards the main channel systems. The internal configuration of the overbank deposits is characterized by thin packages of continuous high amplitude aggradational reflections intercalated by lenticular, chaotic to semi-transparent bodies (Figs. 3 and 4A).

5.2.1.3. Gravitational deposits (MTDs and turbidites).

Gravitational deposits are found mostly as widespread packages or bodies within the dendritic network of channels and along the SW drift flanks (Fig. 5A) or preserved within the gentle slopes of the NE flanks (Figs. 4C and 5C). The dimensions of the gravitational deposits along channel systems vary substantially: between 5 and 10 km in width, 5–50 km in length and 20–100 ms TWT in thickness (Fig. 4A and 4B). The gravitational deposits consist of variable thin-bedded to lenticular bodies (Fig. 4B). In general, thin, sub-parallel, semi-transparent to low amplitude reflections mark turbidites (Fig. 3), whereas thick, lenticular bodies with chaotic, high amplitude or transparent reflections indicate MTDs, such as debrites or slumps near head scarps (Figs. 4 and 5).

The gravitational deposits across the SW drift flanks lie at water depths of approximately 2900–3600 m and have variable shapes (Figs. 4 and 5). They cover an area around 40 km wide and 100 km long, with 3000–5000 km² (up to 27,000 km²), mostly associated with the NE-SW gullies on the SW flanks (Fig. 2). Their internal configurations appear chaotic to wavy, with high amplitude to semi-transparent reflections of unconfined variable shapes (Fig. 5B). Sub-parallel undisturbed, low to high amplitude reflections with a basal discontinuity correspond to slides, whereas deformed, low amplitude to semi-transparent chaotic reflections usually indicate slumps (Fig. 5B).

Gravitational deposits on the NE drift flanks are less common and are usually preserved along gentle steps on the proximal flanks at water depths of 3000–3400 m (Fig. 5C). These deposits are associated with arcuate scarps (Fig. 2) that trend oblique (N-S or NNE-SSW) to the main drift crests and channel systems (NW-SE). On average, the gravitational deposits on the NE flanks have a total thickness of 20–80 ms TWT and cover an area around 10–40 km wide by 30–90 km long (Fig. 5B). Here, they display lenticular shapes with a concave upper surface, characterized by high amplitude, discontinuous sub-parallel reflections interbedded with chaotic semi-transparent bodies (Fig. 5C).

5.2.2. Erosional features

5.2.2.1. Large trunk channels.

Twelve large NW-SE trunk channels represent the largest erosional features in the study area (Fig. 2). The channels are observed between 2500 and 4000 m water depth and are incised by up to 300 m in respect to the surrounding seafloor (Fig. 2). They are 6–15 km wide, 200–400 km long, and their floor dips seaward by 0–1° (Fig. 2). They extend down-slope from the junction (knickpoint) of a dendritic tributary network and form single, wide flat U-shaped features with low sinuosity (Fig. 2). The trunk channels have 2–3 main inflections along their curvature, which are found near the proximal drift flanks, or where they become less confined, seaward of the mounded drifts (Fig. 2). Their internal configuration is interpreted as channel fill, characterized by numerous gravitational deposits with irregular, high amplitude to transparent packages of onlapping, high amplitude, continuous and generally parallel aggrading reflections (Fig. 5A). The thickness of the channel fill that could be imaged in the TOPAS profiles ranges from 50 to 100 ms TWT (Fig. 5A). The trunk channels widen, and their amplitude decreases below ca. 3600–4000 m water depth on the lower continental rise, where they become poorly confined U-shaped features (Fig. 2). The seaward termination of the Tula channel system coincides with the S*E*-NW oriented Tula Fracture Zone (TFZ) (Fig. 2).

5.2.2.2. Channels.

A dendritic network of channels starts at the lower continental slope and continues along the transition to the continental rise at 2500 m water depth (Fig. 2), shaping the proximal parts of the mounded drifts, especially on their SE flanks. The channels exhibit a variety of trends, generally perpendicular (NE-SW) or oblique (N-S or E-W) to the main orientation (NW-SE) of the trunk channels and mounded drifts (Fig. 2). The channels exhibit low to medium sinuosity and form gentle erosional features with 2–7° dip (Fig. S1). They are on average <

100 m deep, 1–3 km wide and 20–80 km long (Fig. 2). Channels also develop down-slope from smaller <1 km wide tributary channels or gullies found on the steep SW drift flanks and on the proximal SE flanks (Fig. 2).

5.2.2.3. Scarps. Several scarps formed by gravitational mass movements are prominent across the proximal parts of the drifts, particularly along their SE and SW flanks, although they can also occur on the NE flanks (Fig. 2). The scarps exhibit concave arcuate shapes, oblique or parallel to the NE-SW margin trend (Fig. 2). Furthermore, these scarps may be associated with normal faults, especially near the large trunk channels (Figs. 4B and 5A), where frequent slope instabilities occur. Their average gradient is 3–8° (Fig. S1), their height 50–100 m, and their width 4–45 km. Scarps in Drifts 6 and 7 occur in a step-like pattern (Fig. 2). The internal configuration of the sediments either side of them is characterized by truncated high amplitude reflections at the headwall and chaotic, irregular to semi-transparent MTDs at the base (Fig. 3).

5.2.3. Mixed features

5.2.3.1. Gullies. The continental slope is marked by numerous gullies —from 550 m water depth near the shelf break to 1600 m water depth on the middle slope (Fig. 2). The gullies appear at the shelf break and are more frequent and deeper incised on the slope beyond the mouth of the cross-shelf troughs, and trend perpendicular to the margin as generally parallel, linear V-shaped features (Fig. 2), which become more U-shaped further down-slope. Gullies also incise the proximal and/or steep flanks of the drifts on the continental rise (Figs. 4 and S1B). These gullies are on average 100 m deep, 500 m wide and dip by 2–5° (Fig. S1). The seismic facies of the seabed on either side of the gullies is characterized by high to low amplitude discontinuous, wavy or convex reflections that end in toplap or truncation against the gullies (Fig. 3).

6. Chronological framework

The correlation between the drill core data from Site 1096 and the sub-bottom profiles allowed us to assign ages to the main seismic units (U1 – U4) and discontinuities (D1 – D4) (Fig. 6B-E). We also evaluated the specific timing of the dominant depositional processes that shaped the continental margin by comparing our discontinuities and depositional evolution with previous chronostratigraphic interpretations of the PMAP (Fig. 7; Rebesco et al., 1996, 1997, 2002; Hernández-Molina et al., 2017). Based on these chronostratigraphic constraints, seismic unit U4 has an age of 1.3–1 Ma, U3 an age of 1–0.6 Ma, U2 an age of 0.6–0.2 Ma, and U1 an age of 0.2–0 Ma (Fig. 7).

7. Discussion

7.1. Depositional model of the Antarctic Peninsula mixed systems

The distribution of the morphological elements and the seismic stacking patterns seen in the high-resolution TOPAS data confirm the depositional model (Fig. 8) initially proposed by Rebesco et al. (1998, 2002) and later revised by Hernández-Molina et al. (2017), which was exclusively based on low-resolution 2D reflection seismic data. In this model, giant drift deposits and complex channel networks developed across the upper to middle continental rise (Fig. 2) and their formation involved interactions between hemipelagic, gravitational and bottom current processes (Lucchi et al., 2002; Lucchi and Rebesco, 2007). The sedimentary products (seismic facies and geometries) observed in the TOPAS sub-bottom profiles further support these interpretations, thereby additionally showing spatial and temporal variations across U1 to U4 (Figs. 4 and 5) that reflect changes in current velocity, frequency, direction, effective range and persistence over time.

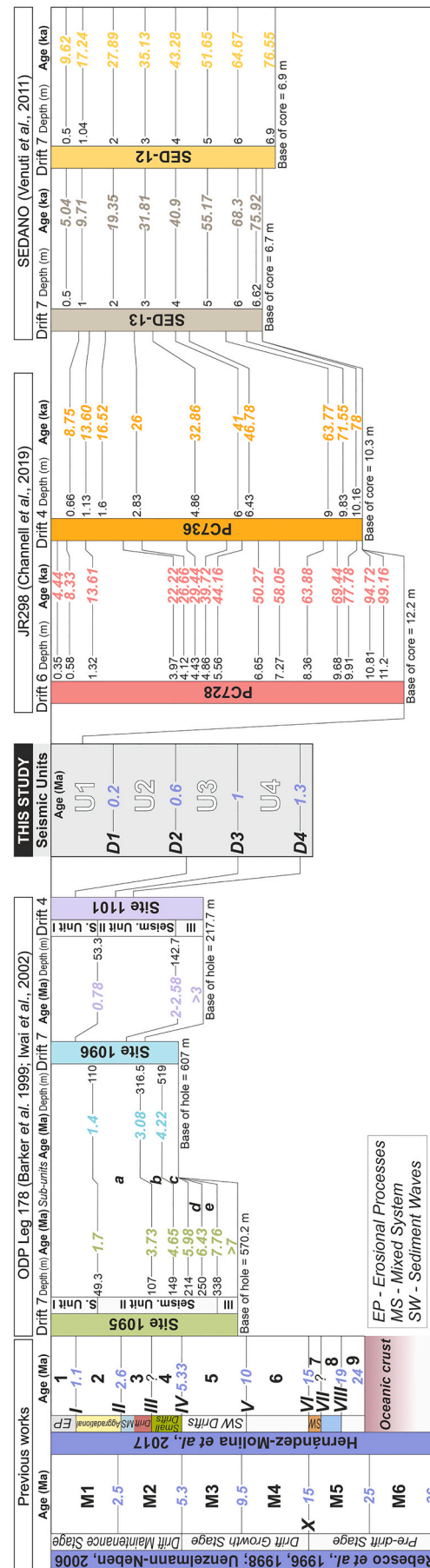Previous studies have concluded that sediment-laden, down-slope

Fig. 7. Chronostratigraphic constraints provided by previous studies (Rebesco et al., 1996, 1998; Uenzelmann-Neben, 2006; Hernández-Molina et al., 2017), ODP Leg 178 Sites (Barker et al., 1999; Iwai et al., 2002), JR298 cores (Channell et al., 2019) and SEDANO cores (Venuti et al., 2011). For ODP Leg 178, correlation lines mark the base of each seismostratigraphic unit and the respective age at each site.
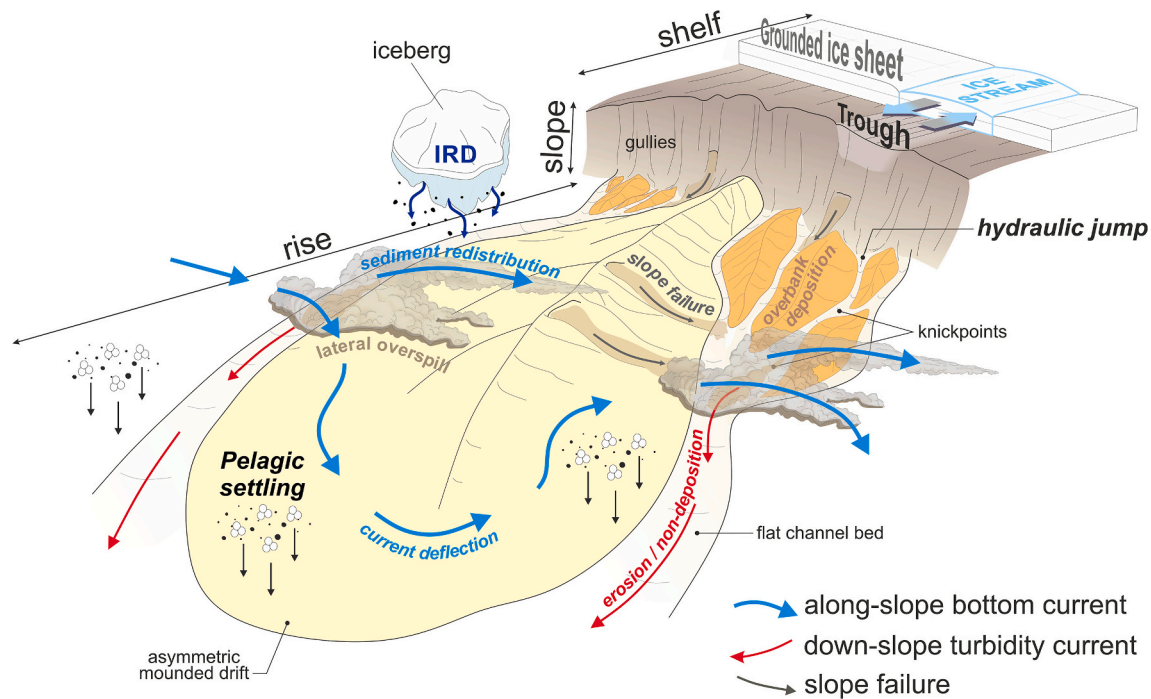
Fig. 8. Conceptual model for the lateral and vertical variations of the mixed depositional systems along the Antarctic Peninsula, modified from Rebesco et al. (1998, 2002) and Hernández-Molina et al. (2017).

turbidity currents acted as the main sediment supplier for the PMAP mixed systems (Fig. 8). The turbidity currents originated mainly from glaciogenic debris that had accumulated at the mouths of cross-shelf troughs during glacial periods when grounded ice streams had advanced through these troughs towards the continental shelf edge (Larter and Cunningham, 1993; Rebesco et al., 1996, 1998, 2002; Barker et al., 1999, 2002; Pudsey, 2000; Amblas et al., 2006; Bart et al., 2007; Hernández-Molina et al., 2017). Hyperpycnal flows from meltwater processes are also considered as an additional sediment source (Lucchi et al., 2002), as ice sheet melting would provide sediment to the proximal shelf and upper slope, similar to other polar continental margins (Hesse et al., 1997; Lucchi et al., 2013). As a result, the turbidity currents / hyperpycnal flows accelerate down-slope, favoured by the steep continental slope morphology (Fig. S1). The abrupt change in gradient at the base of the slope would cause a hydraulic jump (Fig. 8), resulting in deposition of sediments along the proximal channel-complex systems (Fig. 4A), as proposed by Pudsey and Camerlenghi (1998) for the PMAP and Wright and Anderson (1982) for other parts of the Antarctic continental margin. This effect changes the velocity and density conditions, causing deceleration of the turbidity currents and an increase in their overall thickness (Rebesco et al., 2002; Postma et al., 2009; Shanmugam, 2016). Part of the sediment load carried by the turbidity currents more than likely overspills laterally and settles over the low relief of the channel network, thereby building the intra-channel overbank deposits observed in the TOPAS data (Fig. 4A), while the rest of the flow must continue its down-slope movement (Fig. 8). According to the previous depositional model (Rebesco et al., 1998, 2002; Hernández-Molina et al., 2017), the turbidity current would meet the SW-flowing bottom current and synchronous interactions would allow entrainment of the suspended fine-grained particles and redistribution towards the SW (cf. Hillenbrand and Ehrmann, 2001, 2005) (Fig. 8). The turbidity current, deprived of the fine-grained fraction, deposits its coarser load as it slows down (Postma et al., 2009; Shanmugam, 2016), forming gravitational deposits with chaotic seismic facies along the large trunk channels (Fig. 5A), which correspond to sand-rich turbidites and MTDs in marine sediment cores (Lucchi et al., 2002; Lucchi and Rebesco, 2007). The TOPAS profiles also show MTDs across the channel systems and on the

proximal flanks of the mounded drifts (Fig. 4A and 4B), suggesting that occasional gravitational flows may also cause local erosion sediment instabilities along the dendritic channels and adjacent deposits (Fig. 8).

This sedimentary model also assumes that the convergence of the channel network towards a main knickpoint at the onset of the main trunk channel (Fig. 8) causes another hydraulic jump and local deceleration of the turbidity current (Mutti et al., 2009; Shanmugam, 2016). As a result, some of the suspension load would be deposited at the initial channel head due to the seafloor's morphological change (Fig. 2), but most of the coarser high-density flows would bypass the upper continental rise and their particles would settle when the flows become unconfined along the channel thalweg (Lucchi et al., 2002), or when they lose velocity near the channel mouth on the lower continental rise and further seaward on the abyssal plain (Mutti and Normark, 1987; Liu et al., 2013, 2018; Shanmugam, 2016).

Most modern oceanographic and paleoceanographic studies concluded that the bottom current along the PMAP is generally weak and persistent, despite having a fluctuating hydrodynamic regime (Camerlenghi et al., 1997; Pudsey and Camerlenghi, 1998; Pudsey, 2002; Giorgetti et al., 2003; Hillenbrand et al., 2021). Current meter measurements from the central part of Drift 7 showed that the modern bottom current closely follows the bathymetric contours of the mounded drifts near the seafloor and up to 60 m above it, while the main water mass (modified LCDW originating from the Weddell Sea) flows towards the SW (Fig. 1A; Camerlenghi et al., 1997; Giorgetti et al., 2003; Hillenbrand et al., 2008; Hernández-Molina et al., 2017). The bottom current tends to be deflected in a W to NW-ward direction when it encounters the high relief of a mounded drift (Fig. 8) and redistributes the fine-grained particles along the gentle slopes of its NE flank (Camerlenghi et al., 1997; Giorgetti et al., 2003; Rebesco et al., 2007). The bottom current deflects towards the SW again when it has passed the distal drift flank (Fig. 8; Camerlenghi et al., 1997; Giorgetti et al., 2003). Sediment deposition across the drifts has caused alternations between low and high amplitude seismic facies along the NE flanks and crests of the mounded drifts (Figs. 4C and 5B). Along with the presence of MTDs and turbidites at the bases of U3 to U1 (Figs. 4A and 5C), these alternations suggest temporal changes in both the supply of detritus (as the

paleo-ice streams delivered terrigenous debris mainly during glacial periods) and in the bottom current velocity (as the increase in seismic amplitude and acoustic stratification towards the top of the seismic units supports reworking and winnowing of the previously deposited sediments).

Research undertaken across turbidite depositional systems have shown that these systems are characterized by cycles of sediment bypass, erosion, and deposition due to switches between active and dormant phases (Hubbard et al., 2014). When the turbiditic system of the PMAP was dormant, hemipelagic sediments and meltwater plumites were deposited across the margin under the influence of a weak to moderate bottom current (Fig. 8; Pudsey and Camerlenghi, 1998; Hill-enbrand and Ehrmann, 2001, 2005; Lucchi et al., 2002, Lucchi and Rebesco, 2007; Cowan et al., 2008; Vautravers et al., 2013). These depositional processes usually smoothened the overall morphology on the continental rise by covering the seafloor under a drape (Fig. 5C). However, when the turbidity currents were active, amalgamated fine- to coarse-grained turbidites (Lucchi et al., 2002; Lucchi and Rebesco, 2007) were deposited on the channel banks by lateral overspill (Fig. 4A and 4B). At that point, synchronous interaction with the SW-flowing bottom current occurred. Even though this interaction may have been short lived, entrainment of the fine-grained particles suspended in the turbidity currents into the bottom current contributed to the asymmetric growth of the mounded drifts through sediment accumulation along their NE flanks (which show higher thicknesses than the SW flanks, usually >150 ms TWT; Fig. 5B). The switch between active and dormant turbidity phases is most likely responsible for the shift between synchronous and asynchronous interactions with the along-slope current, resulting in intercalations of turbidites, contourites and hemipelagic deposits along inter-channel areas and across the mounded drifts (Fig. 8).

According to our results, turbidity currents are the dominant factor for erosion and deposition across the dendritic channel networks, whose morphology they formed, while bottom currents have a stronger but —despite their nearly permanent flow along the continental margin— variable influence on deposition and erosion and fluctuate along the mounded drifts (Fig. 8). At the time of deposition, sediment particles would be affected by the most dominant process; however, the persistence of bottom currents ultimately leads to redistribution and reworking of most sediments, and especially of fine grains that are still being carried in suspension or exposed at the seafloor surface (Fig. 8).

7.2. Sedimentary evolution of the mixed depositional systems

Four evolutionary stages were identified for the Pleistocene record (Fig. 9): *1.3–1 Ma, 1–0.6 Ma, 0.6–0.2 Ma* and *0.2 – present.*

a) *1.3–1 Ma*

The earliest stage of evolution documented in this study occurred from 1.3–1 Ma, with the deposition of aggradational, uniform sheets (U4) over the pre-existing mounded drift and channel morphologies across the continental rise (Fig. 4B). The lack of gravitational deposits along the channel-complex systems (Fig. 4B) suggests that gravitational processes (turbidity flows and mass-transport processes) were dormant or subordinate (i.e., minor events) during the deposition of U4 (Fig. 9A). As a consequence, along-slope bottom currents and pelagic settling were the dominant processes active at that time forming the thickest, aggradational unit (Fig. 5B). Given that U4 settled over the previous mounded drift and channel morphologies (Fig. 4B), their reliefs and shapes are fully preserved (Rebesco et al., 1997). At Sites 1096 and 1101 on Drifts 7 and 4, respectively, this unit comprises structureless / bioturbated foraminifera- and diatom-bearing clays and silty clays intercalated with terrigenous laminated clays and silts (Fig. 6C and 6F), supporting an along-slope dominated stage (Barker et al., 1999). Bottom current velocities of 5–20 cms^{-1} (McCave, 2008; McCave et al., 2017), similar to

those presently observed (Camerlenghi et al., 1997; Giorgetti et al., 2003), would have been sufficient to capture and redistribute the fine clay and silt particles carried as suspension load in the nepheloid layer and by pelagic fallout (McCave, 2008; Brackenridge et al., 2018; de Castro et al., 2020, de Castro et al., 2021).

b) *1–0.6 Ma*

The period from 1 to 0.6 Ma is marked by local erosion of the previous deposits (U4) (Fig. 5A), with sedimentation of new aggradational sheeted deposits over the mounded drifts and gravitational down-slope deposits across inter-channel areas, over the steep SW flanks, and proximal NE flanks of the mounded drifts (Fig. 4A). This deposition pattern indicates an overall activation of turbidity flows across the channel systems (Fig. 9B).

During U3 deposition, the turbidites along the flanks of the mounded drifts transition laterally and vertically into aggradational sheets with high amplitude (Fig. 4B), suggesting that the fine fraction of the turbidity flows was effectively captured by an along-slope current before being deposited (cf. Shanmugam et al., 1993; Mulder et al., 2008; Fonnesu et al., 2020). A persistent SW-flowing bottom current would have to cover the entire margin under contouritic and hemipelagic deposition to maintain the shapes of the aggradational deposits (Fig. 5C). Along the PMAP, turbidites and MTDs are usually deposited during glacial maxima (Larter and Cunningham, 1993; Pudsey and Camerlenghi, 1998; Rebesco et al., 1998, 2002; Pudsey, 2000; Lucchi et al., 2002; Hernández-Molina et al., 2017). The accumulation of large amounts of glaciogenic debris at the shelf edge supplied by ice streams would have caused numerous gravitational instabilities, leading to frequent sediment gravity flows and other down-slope mass-transport processes (Diviacco et al., 2006; Rebesco and Camerlenghi, 2008) (Fig. 9B). The observed upward and lateral transition from down-slope to along-slope deposits supports that bottom currents effectively pirated the fine-grained particles carried by the suspension cloud (Fig. 9B). Therefore, U3 marks the start of a period of proactive interplay between reactivated turbidity currents and persistent bottom currents (Fig. 9B). During deposition of U3, a slightly moderate and steady current with an average speed of 15–20 cms^{-1} would have been capable of capturing clay and silt particles from active turbidity currents and build the aggradational sheeted morphologies (Fig. 5B). During this stage, Barker et al. (1999) recorded intercalations of bioturbated silty clays and laminated silty clays (Fig. 6C and 6F) with occasional thin-bedded turbidites at Sites 1095, 1096 and 1101, supporting an interplay between frequent turbidity flows and persistent bottom currents.

Longer (orbital) climatic cycles with a periodicity of ~100 kyr became progressively more dominant during the Mid-Pleistocene Transition (MPT), from ~1.2 to 0.65 Ma (Clark et al., 1999, 2006; Maslin and Ridgwell, 2005; McClymont et al., 2013), and significant falls in global sea-level were recorded around 1–0.9 Ma (Haq et al., 1987; Miller et al., 2005, 2011). These climatic variations can be assumed to have increased the duration of ice-sheet grounding events on the Antarctic shelf (Bartek et al., 1991) and, consequently, amplified the gravitational processes across the margin (Fig. 9B). Several studies from around Antarctica (Escutia et al., 2000; Salabarnada et al., 2018) and other continental margins (Gong et al., 2013, 2016; Fonnesu et al., 2020; Fuhrmann et al., 2020) evoke a persistent along-slope bottom current and frequent interactions with gravitational processes to build the large mounded and sheeted morphologies (Fig. 4B).

c) *0.6–0.2 Ma*

The third stage of evolution occurred from 0.6–0.2 Ma and is represented by seismic unit U2 (Fig. 4B). This stage is characterized by a new episode of localized erosion (D2) (Fig. 5A), accompanied by sedimentation of thick gravitational deposits (Fig. 5C). The gravitational deposits cover the entire continental rise, except the NE flanks of the

mounded drifts and their crests (Fig. 4A). During this stage, aggradational deposition occurred along the crests of the mounded drifts (Fig. 4C). This distribution points to an increased frequent activity of turbidity currents during glacial periods (Fig. 9C) (Rebesco et al., 1998, 2002; Amblas et al., 2006; Hernández-Molina et al., 2017). The along-slope bottom current would have been weaker and less influential (Fig. 9C) since it only formed aggradational deposits across the top of the mounded drifts (Fig. 4C). The aggradational deposits have a cyclic stacking pattern, defined by sub-units U2a to U2d (Fig. 5B1). Such cyclic patterns suggest several reactivations of turbidity currents, followed by stronger along-slope current influence and hemipelagic settling (Rebesco et al., 2002; Uenzelmann-Neben, 2006; Hernández-Molina et al., 2017). Records of Sites 1096 and 1101 support this cyclicity, showing a partially turbiditic succession composed of couplets of silt-rich turbidites, structureless diatom-bearing clays and silts, and laminated clays and silts (Fig. 6C and 6F; Barker et al., 1999). This cyclicity may match the ~100 kyr orbital cycles (Fig. 10), hinting at fluctuating hydrodynamic regimes and turbidite input in tandem with glacial-interglacial changes, modulated by short-range eccentricity (Clausen, 1998; Michels et al., 2001; Bart et al., 2007; Forwick et al., 2015; Salabarnada et al., 2018).

d) 0.2 Ma – present

The final stage was characterized by the deposition of U1 from 0.2–0 Ma (Fig. 5C). This stage is characterized by the accumulation of thin turbidites over the channel network and at the base of drift flanks (Fig. 4A), which gradually transition into aggradational stratified deposits across the mounded drifts and overbank areas (Fig. 5C). This upward change occurs at an intermediate scale (with ~10–15 ms TWT repetitive intervals for sub-units U1a and U1b), resembling the cyclicity of deposition observed in U2 (Fig. 5B1). Therefore, down-slope processes were initially active across the channel systems (Fig. 9), where they triggered turbidity currents (Fig. 4A). Subsequently, the fine-grained particles carried by the turbidity flows were entrained in the along-slope current (Fig. 9D), forming intercalations of fine-grained contourites and/or hemipelagites as aggradational sheets (Fig. 4A). Sediments deposited at ODP Leg 178 drift sites are characterized by alternations of laminated terrigenous clays and silts and structureless / bioturbated clays and silty clays enriched in diatoms and foraminifera (Fig. 6C and 6F), with occasional thin-bedded muddy turbidites, supporting cyclic deposition (Barker et al., 1999). The cyclicity of the deposits once again underlines the importance of glacial-interglacial changes across the PMAP (Bart et al., 2007; Lucchi and Rebesco, 2007; Hernández-Molina et al., 2017). After the MPT, the late Pleistocene period is associated with higher amplitude climatic (Clark et al., 1999, 2006; Maslin and Ridgwell, 2005; McClymont et al., 2013) and eustatic oscillations (Haq et al., 1987; Miller et al., 2005, 2011), resulting in higher sediment supply (Fig. 10). Higher sediment input would have shifted the depositional processes from erosion to net accumulation (Solheim et al., 1996) and favoured the development of aggradational deposits across the PMAP (Fig. 5B and 5C). Gravitational transport processes would have still been prominent across the channel-complex systems (Fig. 9D), since the longer climatic cycles (~100 kyr) would reactivate the turbidity currents during glacial stages (Rebesco et al., 1998, 2002; Bart et al., 2007; Hernández-Molina et al., 2017).

The most recent deposit (U1b) below the present seafloor is an extensive aggradational sheet with few signs of gravitational processes, such as <50 m high scarps, <100 m deep gullies and the presence of thin-bedded turbidites (Figs. 2 and 4). This stage suggests less frequency of turbidity currents and more dominant deposition from the along-slope bottom current and/or by hemipelagic processes (Fig. 9D). The sedimentary records at drill Sites 1095, 1096 and 1101 support this interpretation as the most recent sediments are composed mostly of bioturbated, diatom-bearing silty clays alternating with weakly laminated silty clays (Barker et al., 1999). Considering the thickness of only

25–40 ms TWT for the youngest deposits (Fig. 5C), the bottom current was probably weak but persistent along the margin (Fig. 9D). At present, modified LCDW was detected at 6 to 8 m above the seafloor, flowing around the large mounded drifts (Fig. 1A), with velocities of 4 to 6.2 ± 3.4 cms^{-1} and short-term maximum speeds up to 20 cms^{-1} (Camerlenghi et al., 1997; Giorgetti et al., 2003). Hemipelagic sedimentation at the seafloor comprises structureless silty clays (Fig. 6C and 6F), bioturbated diatom-bearing muds and rare diatomaceous oozes at the ODP Sites (Barker et al., 1999), whereas core PC736 is characterized by a thick sequence of laminated to stratified, partly rippled silty clays overlain by a thin unit of bioturbated, diatom-bearing sandy silty clay near the seafloor surface (Hillenbrand et al., 2021) (Fig. 6D), suggesting a modern depositional system dominated by weak bottom currents and winnowing during the latest Pleistocene and Holocene (see also Pudsey and Camerlenghi, 1998; Lucchi et al., 2002; Lucchi and Rebesco, 2007). Clay mineral data from surface sediments corroborate a generally SW-ward transport direction for the modified LCDW (Hillenbrand and Ehrmann, 2001; Hillenbrand et al., 2021).

7.2.1. Glacial-interglacial changes

The variations throughout the stratigraphic stacking pattern (Fig. 5C) indicate an interplay between active turbidity flows and fluctuating bottom currents. The variability of these processes heightens the challenge of decoding the main controls involved, yet, the cyclicity of the sedimentary record suggests recurrent driving mechanisms at different scales. The deposition of U3 and U2 is characterized by a cyclic repetition of chaotic seismic facies at the base that transitions upward into high amplitude, stratified seismic facies (Fig. 4A1). These variations suggest frequent turbiditic or gravitational input, which is later reworked by strong bottom currents towards the top. Based on our age constraints (Fig. 6), we would expect to see the base of U2 linked to a glacial stage, but it appears to fall into an interglacial stage (Fig. 10), which may result from uncertainties in our age model. Amalgamation or erosion of the sedimentary record could also play a role as occasional high amplitude reflections appear below the chaotic deposits (for example, on the SW flank of Drift 3A; Fig. 4B). Therefore, the transitions from chaotic to stratified seismic facies within units U2 and U3 (Fig. 4A1) are probably related to cyclic processes at a large scale, with a frequency around ~400 kyr (Fig. 10). The cyclicities observed in the seismic record suggest that glacial-interglacial changes may have influenced the sedimentary supply and oceanographic processes acting in the study area (Fig. 10). Glacial-interglacial cycles shifted from a periodicity of 40 kyr to 100 kyr with greater amplitudes during the MPT between ~1.2 and 0.65 Ma (Thunell et al., 1991; Clark et al., 1999, 2006; Davies et al., 2012; McClymont et al., 2013). Therefore, U3 and U2 comprise deposits formed during longer lasting glacial and interglacial periods (Fig. 10). Furthermore, the ~400 kyr cyclicity reflected by U3 and U2 is probably linked to very long climatic fluctuations, i.e., a well-known eccentricity periodicity (Fig. 10).

Seismic units U2 and U1 show the same upward trend at an intermediate scale (with ~10–15 ms TWT intervals), reflected by their sub-units U2a, U2b, U2c, U2d, U1a and U1b (Fig. 5B1). These alternations hint at a secondary cyclicity (Fig. 5B1) with a frequency around ~100 kyr (Fig. 10). Such variations may result from interchangeable interactions between turbidity currents and other mass-transport processes, followed by bottom current reworking and hemipelagic settling. Their internal successions (U2a to U1b) roughly coincide with major glacial stages (Clark et al., 1999, 2006; Maslin and Ridgwell, 2005; McClymont et al., 2013), significant falls in global sea-level (Haq et al., 1987; Miller et al., 2005, 2011) and ~ 100 kyr orbital cycles (Fig. 10). Many studies have shown that the sediments deposited after the MPT are modulated by ~100 kyr Milankovitch cycles (e.g., Pudsey, 2002; Kemp et al., 2010; Elderfield et al., 2012). In ODP Leg 178 cores from Sites 1096 and 1101, a ~ 100 kyr dominant periodicity was identified in the lower part of the holes by spectral analysis of magnetic susceptibility data and Th/K ratios (Lauer-Leredde et al., 2002; Rea et al., 2016),
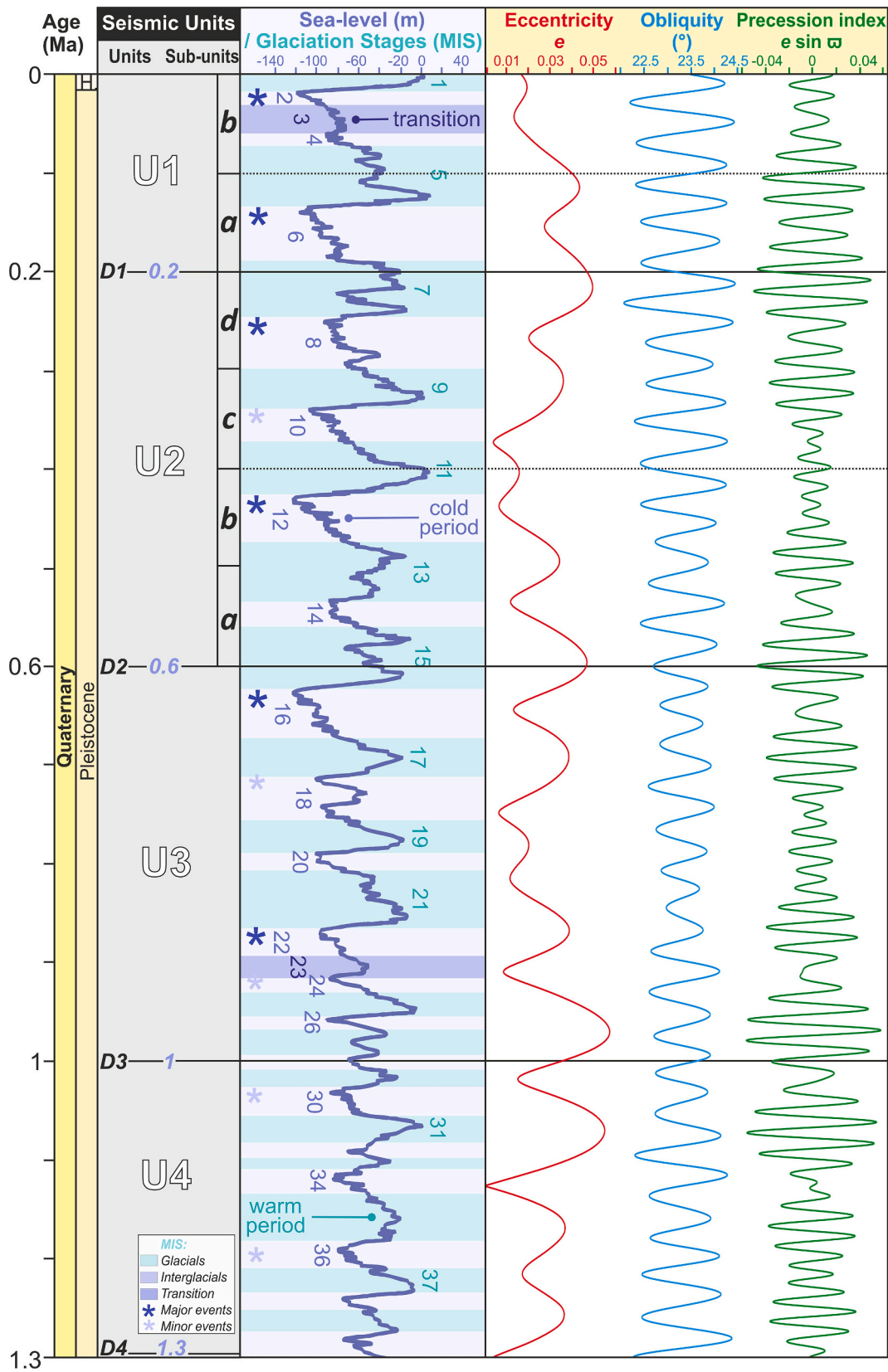
Fig. 10. Evolution of the PMAP mixed systems, marked by glacial-interglacial changes, sea-level fluctuations and orbital forcing. Sea-level curve from Miller et al. (2011), MIS after Lisiecki (2005) and Ogg et al. (2016), and eccentricity, obliquity and precession index from Laskar et al. (2011).

which was preliminarily correlated to orbital eccentricity cycles. Variations in the amount of incident solar energy, ice coverage and volume as well as the Earth's carbon cycle are thus recognized as long-term key drivers of global glacial-interglacial cycles and concomitant environmental changes on the Antarctic continental margin and in the Southern Ocean (e.g., Cowan et al., 2008; Naish et al., 2009; Ito et al., 2010). Changes in the Earth's eccentricity (and/or obliquity and precession over shorter time scales) caused global insolation and climatic variations (Laskar et al., 2004, 2011; Elderfield et al., 2012; Hodell et al., 2013), which ultimately also drove the frequency and strength of along-slope versus down-slope processes across the PMAP and generated cyclic stacking patterns in its depositional record (Fig. 10).

7.3. Implications for other mixed systems

The PMAP mixed systems record lateral and vertical variations of distinct seismic facies and morphological elements, from the asymmetric mounded drifts to the dendritic networks of tributary and main channels (Figs. 4 and 5). This system is further characterized by the presence of secondary erosional and depositional features within the channel systems and along drift flanks (such as MTDs or scarps in Figs. 2 and 3). The morphology of these features is controlled by the most dominant process (i.e., bottom currents or turbidity flows) during and after sediment deposition. Along-slope bottom currents typically form large, mounded drifts through flow stripping of the fine-grained particles during synchronous interactions with turbidity currents and/or through reworking of sediment particles after their deposition. Turbidity currents usually form down-slope channels or channel overbank deposits (Figs. S1 and 3) due to basal erosion and lateral overspill of the turbidity flows, frequently during asynchronous interactions with weak bottom currents (Fig. 8). The dominant process conditions the sedimentary facies formed across each feature (Fig. 8), as well as its extension and thickness over time (Fig. 4B).

Mixed depositional systems with similar morphological elements have been identified on other polar continental margins, both around Antarctica (Escutia et al., 2000; Scheuer et al., 2006; Jiménez-Espejo et al., 2020) and in SE Greenland (Clausen, 1998; Kuijpers et al., 2003). Other studies discovered several mixed or hybrid depositional systems in the Mesozoic and Cenozoic records (Gong et al., 2013, 2016; Mutti et al., 2014; Creaser et al., 2017; Sansom, 2018; Fonnesu et al., 2020). These systems share similar depositional and erosional features, with differences in spatial layout, dimensions, seismic stacking patterns and sedimentary facies. Examples from the Mesozoic include the Late Cretaceous record from the middle slope to the upper rise offshore Uruguay (Creaser et al., 2017) and Argentina (Rodrigues et al., 2021), while Cenozoic examples include the Late Miocene-Quaternary record along the upper slope of the South China Sea (Gong et al., 2013, 2016), the Pliocene record offshore SE Greenland (Rasmussen et al., 2003), and the Paleogene to present deposits along the upper and middle slope of Brazil (Mutti et al., 2014; Pandolpho et al., 2021), Tanzania and Mozambique (Sansom, 2018; Fonnesu et al., 2020; Fuhrmann et al., 2020).

The PMAP mixed systems developed along the lower continental slope and rise (Fig. 2), below a steep upper to middle continental slope (Fig. 3; Rebesco et al., 1998; Dowdeswell et al., 2004). The Late Cretaceous mixed systems along the margins of Uruguay, Argentina and SE Greenland developed below a steep upper slope and extend from the middle slope to the upper continental rise (Rasmussen et al., 2003; Creaser et al., 2017; Rodrigues et al., 2021). These systems are characterized by large asymmetric mounded drifts and channels, which migrate laterally and down-stream of the prevailing bottom current. The PMAP drifts do not show a clear lateral migration in the high-resolution sub-bottom profiles. Rather, the large asymmetric drifts exhibit extensive aggradation with thicknesses of >50–150 ms TWT along the gentle NE flanks and drift crests (Figs. 5B and 6C). However, previous low-resolution reflection seismic studies identified an up-current migration of most drifts crests towards NE (Rebesco et al., 1997, 2002, 2007;

Uenzelmann-Neben, 2006). The PMAP mounded drifts have larger dimensions than other mixed systems, up to ~1 km in thickness, 70–100 km in width and 200–300 km in length (Fig. 2). The Argentine system is on average 300–500 m thick, 10–30 km wide, and 30–75 km long (Rodrigues et al., 2021), whereas on the Uruguayan margin these features reach 800 m in thickness, 10–15 km in width and ~ 50 km in length (Creaser et al., 2017). These systems differ from the PMAP mixed systems in terms of their dimensions and unilateral down-current migration, which could suggest that their lateral migration and asymmetric drifts result from more frequent and synchronous interactions between bottom currents and turbidity flows. The PMAP mixed systems are characterized by extensive channel networks and large mounded drifts (Fig. 2) with vertical transitions from gravitational to aggradational sheeted deposits (Figs. 4 and 5), suggesting less synchronous interactions.

Other mixed systems prograde down-current, such as the Late Miocene-Quaternary deposits of the Pearl River Mouth system in the South China Sea (Gong et al., 2013, 2016). This system comprises short unidirectionally, NE-migrating deep-water channels with NE prograding channel-drifts formed within the channels. On average, the channel-drifts exhibit smaller dimensions with thicknesses of 150–170 m, widths of 2.5–5 km and lengths of 20–25 km (Gong et al., 2013). The presence of prominent erosional surfaces (discontinuities) between the channel-fill turbidites and the channel-drift deposits (Gong et al., 2016) suggests asynchronous interactions between along- and down-slope processes. The PMAP shares similar sedimentary facies within the dendritic channel network (Fig. 4A), with interbedded deposition of amalgamated turbidites along the channel axis and along the terminations of the drifts' flanks (Fig. 4A), which transition into fine-grained sediments along the NE flanks and crests of the drifts (Fig. 4C). However, the PMAP is also characterized by synchronous interactions along the NE drift flanks, marked by a transition from stratified facies towards chaotic facies (Fig. 5A). The mixed systems of the South China Sea therefore point to more active but asynchronous interactions between down- and along-slope processes.

The mixed systems deposited along the upper and middle slopes of the Brazilian, Tanzanian and Mozambique margins (Mutti et al., 2014; Sansom, 2018; Chen et al., 2020; Fonnesu et al., 2020; Fuhrmann et al., 2020; Pandolpho et al., 2021) share similar morphologies with the PMAP systems, despite being located at shallower water depths along the continental margin than those of the PMAP. Their mixed systems feature laterally migrating asymmetric channel-drifts (or channel-levees) and offset stacking sedimentary lobes. These systems prograde up-current, following the channel-belt migration and bottom current direction, which was recently tested by Miramontes et al. (2020). The channel-drifts and lobes are considerably smaller, typically 300 m thick, 10–20 km wide and 35 km long (Sansom, 2017, 2018; Fonnesu et al., 2020). The distinct morphologies indicate a higher turbiditic influence under longer synchronous interaction than on the PMAP. The PMAP mixed systems also differ from the previously mentioned examples not only due to their considerable dimensions (Fig. 2), but also due to their somewhat distinct morphologies and deposits (Figs. 4 and 5). The upward transition from chaotic to stratified seismic facies (Fig. 5C1) and the gradual variations in the reworked deposits (Fig. 8) indicate periods of synchronous to asynchronous interactions between along- and down-slope processes (Fig. 8). However, the PMAP mixed systems are also characterized by turbidites and MTDs interbedded across the channel networks (Fig. 4B), which indicates periods of asynchronous interactions with little influence of along-slope current flow. Overall, the influence of along-slope versus down-slope processes takes precedence over the margin morphology (Fig. 2). Whilst turbidity currents are considered more influential along the channel network, along-slope currents are responsible for shaping the mounded drifts (Fig. 8). In previously proposed models for mixed systems (Mutti et al., 2014; Sansom, 2018; Fonnesu et al., 2020; Miramontes et al., 2020), turbiditic flows across the upper and middle slope are considered the dominant

process, affected by weak, persistent bottom currents. The results presented here suggest that our model and the previous models represent two different types of mixed systems due to the interaction and synchrony between down- and along-slope processes. A mixed system fluctuates across a continuum of transport, depositional and erosional processes, resulting in turbidite-dominated to contourite-dominated deposits. Therefore, we conclude that a mixed system comprises a wide variety of features and deposits formed under synchronous, asynchronous and passive interactions, as recently proposed by Rodrigues et al. (2021) and Miramontes et al. (2021). The term "hybrid systems" should be used when the interactions between the two processes are mostly synchronous in time and space (Rodrigues et al., 2021).

Based on our comparisons, we can further deduce that most mixed systems built along polar margins (PMAP, Wilkes Land, Weddell Sea and SW Greenland) developed across an extensive continental rise and under a steep continental slope (Fig. S1; Rebesco et al., 1996, 1998, 2002; Escutia et al., 2000; Rasmussen et al., 2003). The steep slope separates paleo-ice stream troughs on the continental shelf from the mixed systems on the continental rise (Fig. 2) and transfers detritus through frequent down-slope gravitational processes during glacial maxima (Larter and Cunningham, 1993; Rebesco et al., 1998, 2002; Hernández-Molina et al., 2017). Other processes, such as meltwater plumes, are a secondary sediment source for polar mixed systems (Pudsey and Camerlenghi, 1998; Lucchi et al., 2002; Lucchi and Rebesco, 2007; Amblas et al., 2006; Cowan et al., 2008; Vautravers et al., 2013), because they deliver fine-grained particles that can be easily entrained by the along-slope bottom current during deglacial and interglacial stages (Fig. 9).

Non-polar mixed systems appear to have two distinct margin morphologies, which may have contributed to the extent and location of their morphological features. The first is characterized by a steep upper continental slope, which separates the continental shelf with its sedimentary basins and structural highs from the middle to lower continental slope and continental rise, which host large mixed systems (as observed for the Argentine and Uruguayan mixed systems; Creaser et al., 2017; Rodrigues et al., 2021). This type of mixed system is supported by frequent gravitational processes across the upper slope, which release sediment from >1 km thick sedimentary succession accumulated in the basins towards the deeper mixed systems (Creaser et al., 2017; Rodrigues et al., 2021). The second type of non-polar mixed systems appears to develop across the upper to middle continental slope, below a gentle shelf break (as seen in the South China Sea; Gong et al., 2013, 2016). In this type of mixed systems, the main channels act as pathways for turbidity currents and debris flows flowing through them and receive detritus derived from lateral overspill of neighbouring channels and from through bottom current entrainment. Coarser deposits may accumulate along the channel bed, near knickpoints, confluences or deflections of the channel; however, most high-density turbidity flows will bypass the slope and upper continental rise, and their sediment load settles further seaward as submarine fans (Gong et al., 2013, 2016). The morphologies of these systems are significantly smaller (as shown for the Mozambican and Tanzanian mixed systems (Sansom, 2017, 2018; Fonnesu et al., 2020) as the margin configuration and available accommodation space restricts their development further seaward. Based on this comparison, we can infer that the margin configuration and degree of confinement play significant roles in the development of mixed systems as they affect the extent of their main morphological features and the type of deposit accumulated or preserved within their sedimentary records.
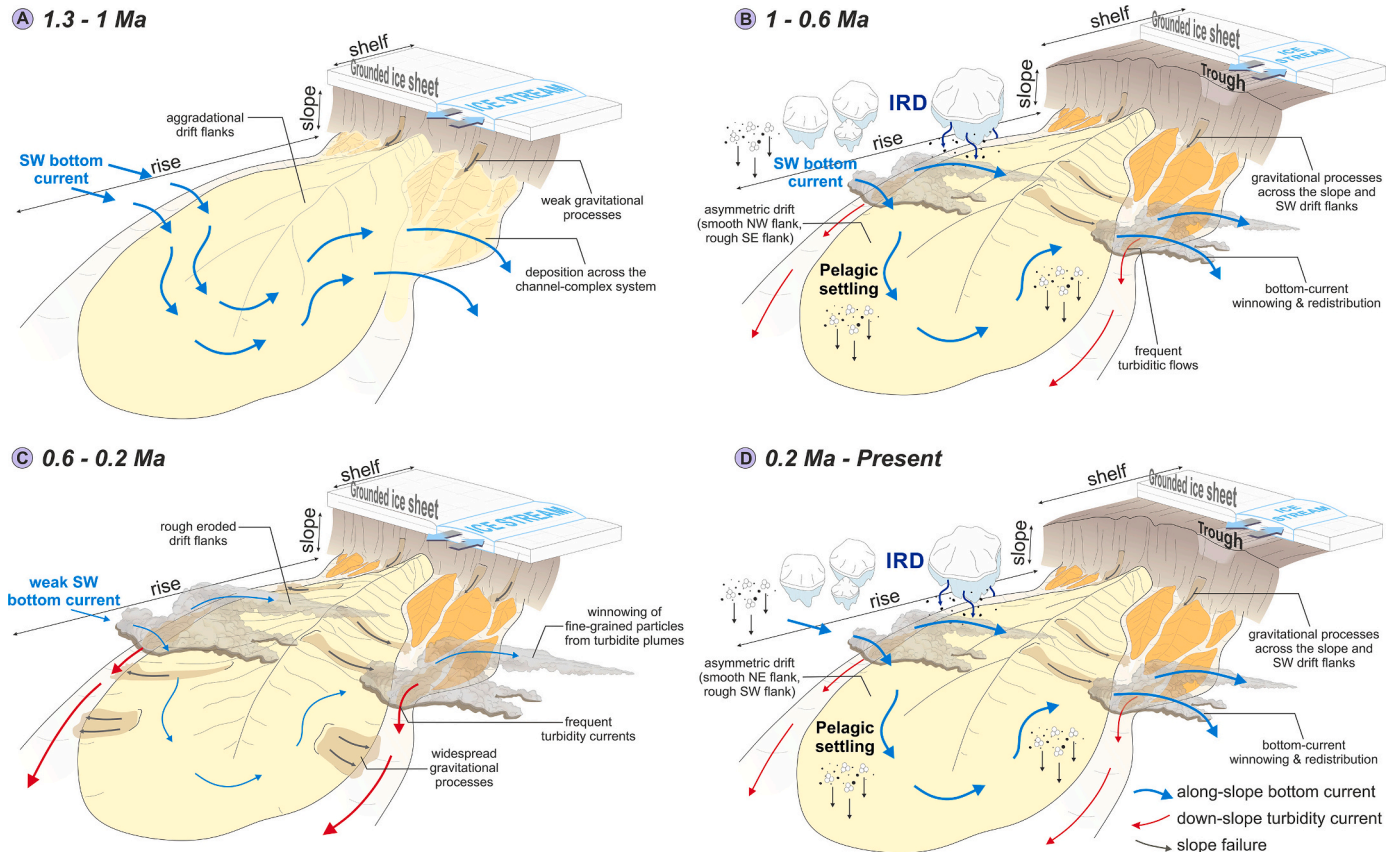

Fig. 9. Representation of the depositional evolution of the PMAP mixed systems, characterized by four distinct stages with changes in body morphology, deposits and driving processes.

8. Conclusions

Mixed depositional systems have been the focus of several studies over recent years. The PMAP mixed depositional systems contain a wide range of features and deposits, developed along the upper to middle continental rise. Our results show greater variability and fluctuations in the seismic facies and in the type of deposit preserved within the sedimentary record of these mixed systems, resulting from ~40 to 100 kyr cyclic changes in glaciogenic sediment supply and bottom current intensity. Erosion followed by sedimentation of gravitational down-slope deposits across the base of most seismic units (U1–U3) points to an increased supply of glaciogenic debris during major glacial periods, whereas an increase in seismic amplitude and stratification towards the top of these units marks an intensification of the SW-flowing bottom current after these periods. Hemipelagic settling and weak bottom current activity are interpreted to have dominated deposition during interglacial periods. In addition, switches between synchronous and asynchronous interactions between the SW-flowing bottom current and the NW-directed down-slope turbidity currents were observed at short to long timescales, which resulted from the impact of glacial-interglacial changes and orbital forcing (eccentricity and obliquity phases) on the interplay of deep-water processes.

The PMAP mixed systems have made a significant contribution to the recognition of mixed depositional systems and provided a deeper understanding of their morphology and spatial variability at a high-resolution vertical scale (>10–150 ms TWT). This study demonstrates that such systems are characterized by intercalations of contourites, thin-bedded turbidites, MTDs and hemipelagites along the down-slope elongated mounded drifts and even across the channel overbank deposits of the complex channel systems. Given the complexity of the mixed systems on the PMAP, which have existed for millions of years and are still active, other modern and ancient examples of mixed systems should be studied, sampled, and compared to improve our understanding of their complexity and to help establish meaningful diagnostic criteria and quantify their main driving processes.

Supplementary data to this article can be found online at https://doi.org/10.1016/j.margeo.2022.106754.

Data Availability Statement

Datasets related to this article can be found at https://doi.org/10.5285/BDFEB69C-DF5C-461D-B7A8-583F9DAAB685 and at https://doi.org/10.5285/836f016a-33be-6ddc-e053-6c86abc0788e, hosted by the UK Polar Data Centre (Larter *et al.*, 2021) and the British Oceanographic Data Centre (GEBCO, 2019).

Declaration of Competing Interest

We declare that we have no commercial or associative aim that might represent a conflict of interest in connection with the work submitted.

References

Acton, G.D., Guyodo, Y., Brachfel, S.A., 2002. Magnetostratigraphy of Sediment rifts on the Continental Rise of West Antarctica (ODP Leg 178, Sites 1095, 1096, and 1101). In: Barker, P.F., Camerlenghi, A., Acton, G.D., Ramsay, A.T.S. (Eds.), Proceedings of the Ocean Drilling Program, ODP, Sci. Res. vol. 178, pp. 1–61. https://doi.org/10.2973/odp.proc.sr.178.235.2002.

Amblas, D., Canals, M., 2016. Contourite drifts and canyon-channel systems on the Northern Antarctic Peninsula Pacific margin. In: Dowdeswell, J.A., Canals, M., Jakobsson, M., Todd, B.J., Dowdeswell, E.K., Hogan, K.A. (Eds.), Atlas of Submarine Glacial Landforms: Modern, Quaternary and Ancient, Geol. Soc. London, Memoirs, 46, pp. 393–394. https://doi.org/10.1144/M46.17.

Amblas, D., Urgeles, R., Canals, M., Calafat, A.M., Rebesco, M., Camerlenghi, A., Estrada, F., De-Batist, M., Hughes-Clarke, J.E., 2006. Relationship between continental rise development and palaeo-ice sheet dynamics, northern Antarctic Peninsula Pacific margin. Quat. Sci. Rev. 25, 933–944. https://doi.org/10.1016/j.quascirev.2005.07.012.

Arndt, J.A., Schenke, H.W., Jakobsson, M., Nitsche, F.O., Buys, G., Goleby, B., Rebesco, M., Bohoyo, F., Hong, J., Black, J., Greku, R., Udintsev, G., Barrios, F., Reynoso-Peralta, W., Taisei, M., Wigley, R., 2013. The International Bathymetric Chart of the Southern Ocean (IBCSO) Version 1.0—a new bathymetric compilation covering circum-Antarctic waters. Geophys. Res. Lett. 40, 3111–3117. https://doi.org/10.1002/grl.50413.

Barker, P.F., Camerlenghi, A., Leg 178 Scientific Party, 1999. ODP Proceedings, Init. Rep. 178. Ocean Drilling Program, College Station, TX, p. 90.

Barker, P.F., Camerlenghi, A., Acton, G.D., Ramsay, A.T.S., 2002. Proceedings of the Ocean Drilling Program, Sci. Res. 178 (CD-ROM). Available from Ocean Drilling Program, Texas A&M University, College Station, TX 77845-9547, U.S.A.

Bart, P.J., Hillenbrand, C.-D., Ehrmann, W., Iwai, M., Winter, D., Warny, S.A., 2007. Are Antarctic Peninsula Ice Sheet grounding events manifest in sedimentary cycles on the adjacent continental rise? Mar. Geol. 236, 1–13. https://doi.org/10.1016/j.margeo.2006.09.008.

Bartek, L.R., Vail, P.R., Anderson, J.B., Emmet, P.A., Wu, S., 1991. Effect of Cenozoic ice sheet fluctuations in Antarctica on the stratigraphic signature of the Neogene. J. Geophys. Res. 96, 6753–6778. https://doi.org/10.1029/90JB02528.

Batchelor, C.L., Bellwald, B., Planke, S., Ottensen, D., Henriksen, S., Myklebust, R., Johansen, S.E., Dowdeswell, J.A., 2021. Glacial, fluvial and contour-current derived sedimentation along the northern North Sea margin through the Quaternary. Earth Planet. Sci. Lett. 566, 1–13. https://doi.org/10.1016/j.epsl.2021.116966.

Brackenridge, R.E., Hernández-Molina, F.J., Stow, D.A.V., Llave, E., 2013. A Pliocene mixed contourite-turbidite system offshore the Algarve Margin, Gulf of Cadiz: seismic response, margin evolution and reservoir implications. Mar. Pet. Geol. 46, 36–50. https://doi.org/10.1016/j.marpetgeo.2013.05.015.

Brackenridge, R.E., Stow, D.A., Hernández-Molina, F.J., Jones, C., Mena, A., Alejo, I., Ducassou, E., Llave, E., Ercilla, G., Nombela, M.A., Pérez-Arlucea, M., Frances, G., 2018. Textural characteristics and facies of sand-rich contourite depositional systems. Sedimentology 65, 2223–2252. https://doi.org/10.1111/sed.12463.

Camerlenghi, A., Crise, A., Pudsey, C.J., Accerboni, E., Laterza, R., Rebesco, M., 1997. Ten-month observation of the bottom current regime across a sediment drift of the Pacific margin of the Antarctic Peninsula. Antarct. Sci. 9, 426–433. https://doi.org/10.1017/S0954102097000552.

Canals, M.R., Urgeles, R., Calafat, A.M., 2000. Deep sea-floor evidence of past ice streams off the Antarctic Peninsula. Geology 28, 31–34. https://doi.org/10.1130/0091-7613(2000)028<0031:DSEOPI>2.0.CO;2.

Carlson, R.L., Gangi, A.F., Snow, K.R., 1986. Empirical reflection travel time versus depth and velocity versus depth functions for the deep-sea sediment column. J. Geophys. Res. 91, 8249–8266. https://doi.org/10.1029/JB091iB08p08249.

Carter, L., McCave, I.N., Williams, M.J.M., 2009. Circulation and water masses of the Southern Ocean: A review. In: Florindo, F., Siegert, M. (Eds.), Antarctic Climate Evolution. Dev. Earth Environm. Sci, 8. Elsevier, pp. 85–114. https://doi.org/10.1016/S1571-9197(08)00004-9.

Catuneanu, O., Abreu, V., Bhattacharya, J.P., Blum, M.D., Dalrymple, R.W., Eriksson, P. G., Fielding, Christopher R., Fisher, W.L., Galloway, W.E., Gibling, M.R., Giles, K.A., Holbrook, J.M., Jordan, R., Kendall, C.G., Macurda, B., Martinsen, O.J., Miall, A.D., Neal, J.E., Nummedal, D., Pomar, L., Posamentier, H.W., Pratt, B.R., Sarg, J.F., Shanley, K.W., Steel, R.J., Strasser, A., Tucker, M.E., Winker, C., 2009. Towards the standardization of sequence stratigraphy. Earth Sci. Rev. 92, 1–33. https://doi.org/10.1016/j.earscirev.2008.10.003.

Channell, J.E.T., Xuan, C., Hodell, D.A., Crowhurst, S.J., Larter, R.D., 2019. Relative paleointensity (RPI) and age control in Quaternary sediment drifts off the Antarctic

Peninsula. Quat. Sci. Rev. 211, 17–33. https://doi.org/10.1016/j. quascirev.2019.03.006.

Chen, Y., Yao, G., Wang, X., Lv, F., Shao, D., Lu, Y., Cao, Q., Tang, P., 2020. Flow processes of the interaction between turbidity flows and bottom currents in sinuous unidirectionally migrating channels: an example from the Oligocene channels in the Rovuma Basin, offshore Mozambique. Sediment. Geol. 404, 105680 https://doi.org/10.1016/j.sedgeo.2020.105680.

Clark, P.U., Alley, R.B., Pollard, D., 1999. Northern hemisphere ice-sheet influences on global climate change. Science 286, 1104–1111.

Clark, P.U., Archerb, D., Pollard, D., Blumd, J.D., Riale, J.A., 2006. The middle Pleistocene transition: characteristics, mechanisms, and implications for long-term changes in atmospheric pCO2. Quat. Sci. Rev. 25, 3150–3184. https://doi.org/10.1016/j.quascirev.2006.07.008.

Clausen, L., 1998. The Southeast Greenland glaciated margin: 3D stratal architecture of shelf and deep sea. In: Stoker, M., Evans, D., Cramp, A. (Eds.), Geological Processes on Continental Margins: Sedimentation, Mass-Wasting and Stability, Geol. Soc. London Spec. Publ, vol. 129, pp. 173–203. https://doi.org/10.1144/GSL.SP.1998.129.01.12.

Cowan, E.A., Hillenbrand, C.-D., Hassler, L.E., Ake, M.T., 2008. Coarse-grained terrigenous sediment deposition on continental rise drifts: a record of Plio-Pleistocene glaciation on the Antarctic Peninsula. Palaeogeogr. Palaeoclimatol. Palaeoecol. 265, 275–291. https://doi.org/10.1016/j.palaeo.2008.03.010.

Creaser, B., Hernández-Molina, F.J., Badalini, G., Thompson, P., Walker, R., Soto, M., Conti, B., 2017. A Late Cretaceous mixed (turbidite-contourite) system along the Uruguayan Margin: sedimentary and palaeoceanographic implications. Mar. Geol. 390, 234–253. https://doi.org/10.1016/j.margeo.2017.07.004.

Davies, B.J., Hambrey, M.J., Smellie, J.L., Carrivick, J.L., Glasser, N.F., 2012. Antarctic Peninsula Ice Sheet evolution during the Cenozoic Era. Quat. Sci. Rev. 31, 30–66. https://doi.org/10.1016/j.quascirev.2011.10.012.

de Castro, S., Hernández-Molina, F.J., Rodríguez-Tovar, F.J., Llave, E., Ng, Z.L., Nishida, N., Mena, A., 2020. Contourites and bottom current reworked sands: bed facies model and implications. Mar. Geol. 428, 106267 https://doi.org/10.1016/j.margeo.2020.106267.

de Castro, S., Hernández-Molina, F.J., de Weger, W., Jiménez-Espejo, F.J., Rodríguez-Tovar, F.J., Mena, A., Llave, E., Sierro, F.J., 2021. Contourite characterization and its discrimination from other deep-water deposits in the Gulf of Cadiz contourite depositional system. Sedimentology. https://doi.org/10.1111/sed.12813.

Dinniman, M.S., Klinck, J.M., Smith Jr., W.O., 2011. A model study of Circumpolar Deep Water on the West Antarctic Peninsula and Ross Sea continental shelves. Deep-Sea Res. Part II 58 (1–3), 1508–1523. https://doi.org/10.1016/j.dsr2.2010.11.013.

Diviacco, P., Rebesco, M., Camerlenghi, A., 2006. Late Pliocene mega debris flow deposit and related fluid escapes identified on the Antarctic Peninsula continental margin by seismic reflection data analysis. Mar. Geophys. Res. 27, 109–128. https://doi.org/10.1007/s11001-005-3136-8.

Donohue, K.A., Tracey, K.L., Watts, D.R., Chidichimo, M.P., Chereskin, T.K., 2016. Mean Antarctic circumpolar current transport measured in drake passage. Geophys. Res. Lett. 43, 760–767. https://doi.org/10.1002/2016GL070319.

Dowdeswell, J.A., Ó Cofaigh, C., Evans, J., 2004. Continental slope morphology and sedimentary processes at the mouth of an Antarctic palaeo-ice stream. Mar. Geol. 204, 203–214. https://doi.org/10.1016/S0025-3227(03)00338-4.

Elderfield, H., Ferretti, P., Greaves, M., Crowhurst, S., McCave, I.N., Hodell, D., Piotrowski, A.M., 2012. Evolution of ocean temperature and ice volume through the Mid-Pleistocene climate transition. Science 337, 704–709. https://doi.org/10.1126/science.1221294.

Escutia, C., Eittreim, S.L., Cooper, A.K., Nelson, C.H., 2000. Morphology and acoustic character of the Antarctic Wilkes Land turbidite systems: ice-sheet-sourced versus river-sourced fans. J. Sediment. Res. 70, 84–93. https://doi.org/10.1306/2DC40900-0E47-11D2-8643000102C1865D.

Faugères, J.-C., Stow, D.A.V., Imbert, P., Viana, A.R., 1999. Seismic features diagnostic of contourite drifts. Mar. Geol. 162, 1–38. https://doi.org/10.1016/S0025-3227(99)00068-7.

Fonnesu, M., Palermo, D., Galbiati, M., Marchesini, M., Bonamini, E., Bendias, D., 2020. A new world-class deep-water play-type, deposited by the syndepositional interaction of turbidity flows and bottom currents: the giant Eocene Coral Field in northern Mozambique. Mar. Pet. Geol. 111, 179–201. https://doi.org/10.1016/j.marpetgeo.2019.07.047.

Forwick, M., Laberg, J.S., Hass, H.C., Osti, G., 2015. The Kongsfjorden Channel System offshore NW Svalbard: downslope sedimentary processes in a contour-current-dominated setting. Arktos 1. https://doi.org/10.1007/s41063-015-0018-4.

Fuhrmann, A., Kane, I.A., Ferguson, R.A., Schomacker, E., Bonamini, E., Contreras, F.A., 2020. Hybrid turbidite-drift channel complexes: an integrated multiscale model. Geology 48. https://doi.org/10.1130/G47179.1.

Gales, J.A., Forwick, M., Laberg, J.S., Vorren, T.O., Larter, R.D., Graham, A.G.C., Baeten, N.J., Amundsen, H.B., 2013. Arctic and Antarctic submarine gullies – a comparison of high latitude continental margins. Geomorphology 201, 449–461. https://doi.org/10.1016/j.geomorph.2013.07.018.

García, M., Ercilla, G., Alonso, B., Estrada, F., Jané, G., Mena, A., Alves, T., Juan, C., 2015. Deep-water turbidite systems: a review of their elements, sedimentary processes and depositional models. Their characteristics on the Iberian margins. Bol. Geol. Min. 126, 189–218.

General Bathymetric Chart of the Oceans, . GEBCO 2019 Grid. Available online at. www. gebco.net. https://doi.org/10.5285/836f016a-33be-6ddc-e053-6c86abc0788e.

Giorgetti, G., Crise, A., Laterza, R., Perini, L., Rebesco, M., Camerlenghi, A., 2003. Water masses and bottom boundary layer dynamics above a sediment drift of the Antarctic Peninsula Pacific Margin. Antarct. Sci. 15, 537–546. https://doi.org/10.1017/S0954102003001652.

Gong, C., Wang, Y., Zhu, W., Li, W., Xu, Q., 2013. Upper Miocene to Quaternary unidirectionally migrating deep-water channels in the Pearl River Mouth Basin, northern South China Sea. AAPG Bull. 97, 285–308. https://doi.org/10.1306/07121211159.

Gong, C., Wang, Y., Zheng, R., Hernández-Molina, F.J., Li, Y., Stow, D.A.V., Xu, Q., Brackenridge, R., 2016. Middle Miocene reworked turbidites in the Baiyun Sag of the Pearl River Mouth Basin, northern China Sea margin: processes, genesis, and implications. J. Asian Earth Sci. 128, 116–129. https://doi.org/10.1016/j.jseaes.2016.06.025.

Gong, C., Steel, R.J., Wang, Y., 2020. Channel-Levee Evolution in Combined Contour Current-Turbidity Current Flows from Flume Tank Experiments [Forum Comment: Geology]. https://doi.org/10.1130/G47508C.1.

Haq, B.U., Hardenbol, J., Vail, P.R., 1987. Chronology of fluctuating sea levels since the Triassic. Science 235, 1156–1167. https://doi.org/10.1126/science.235.4793.1156.

Haughton, P., Davis, C., McCaffrey, W., Barker, S., 2009. Hybrid sediment gravity flow deposits – Classification, origin and significance. Mar. Pet. Geol. 26, 1900–1918. https://doi.org/10.1016/j.marpetgeo.2009.02.012.

Hernández-Molina, F.J., Larter, R.D., Rebesco, M., Maldonado, A., 2006. Miocene reversal of bottom water flow along the Pacific Margin of the Antarctic Peninsula: stratigraphic evidence from a contourite sedimentary tail. Mar. Geol. 228, 93–116. https://doi.org/10.1016/j.margeo.2005.12.010.

Hernández-Molina, F.J., Larter, R.D., Maldonado, A., 2017. Neogene to Quaternary stratigraphic evolution of the Antarctic Peninsula, Pacific Margin offshore of Adelaide Island: transitions from a non-glacial, through glacially-influenced to a fully glacial state. Glob. Planet. Chang. 156, 80–111. https://doi.org/10.1016/j.gloplacha.2017.07.002.

Heroy, D.C., Anderson, J.B., 2005. Ice-sheet extent of the Antarctic Peninsula region during the Last Glacial Maximum (LGM) – Insights from glacial geomorphology. Geol. Soc. Am. Bull. 117, 1497–1512. https://doi.org/10.1130/B25694.1.

Hesse, R., Khodabakhsh, S., Klaucke, I., Ryan, W.B.F., 1997. Asymmetrical turbid surface-plume deposition near ice-outlets of the Pleistocene Laurentide ice sheet in the Labrador Sea. Geo-Mar. Lett. 17, 179–187. https://doi.org/10.1007/s003670050024.

Hillenbrand, C.-D., Ehrmann, W., 2001. Distribution of clay minerals in Drift Sediments on the Continental rise West of the Antarctic Peninsula, ODP Leg 178, Sites 1095, 1096, and 1101. In: Barker, P.F., Camerlenghi, A., Acton, G.D., Ramsay, A.T.S. (Eds.), Proceedings of Ocean Drilling Program, Sci. Res, vol. 178, pp. 1–33. https://doi.org/10.2973/odp.proc.sr.178.224.2001.

Hillenbrand, C.-D., Ehrmann, W., 2005. Late Neogene to Quaternary environmental changes in the Antarctic Peninsula region: evidence from drift sediments. Glob. Planet. Chang. 45, 165–191. https://doi.org/10.1016/j.gloplacha.2004.09.006.

Hillenbrand, C.-D., Camerlenghi, A., Cowan, E.A., Hernández-Molina, F.J., Lucchi, R.G., Rebesco, M., Uenzelmann-Neben, G., 2008. The present and past bottom-current flow regime around the sediment drifts on the continental rise west of the Antarctic Peninsula. Mar. Geol. 255, 55–63. https://doi.org/10.1016/j.margeo.2008.07.004.

Hillenbrand, C.-D., Crowhurst, S.J., Williams, M., Hodell, D.A., McCave, I.N., Ehrmann, W., Xuan, C., Piotrowski, A.M., Hernández-Molina, F.J., Graham, A.G.C., Grobe, H., Williams, T.J., Horrock, J.R., Allen, C.S., Larter, R.D., 2021. New insights from multi-proxy data from the West Antarctic continental rise: Implications for dating and interpreting Late Quaternary palaeoenvironmental records. Quat. Sci. Rev. 257 (106842), 1–25. https://doi.org/10.1016/j.quascirev.2021.106842.

Hodell, D., Crowhurst, S., Skinner, L., Tzedakis, P.C., Margari, V., Channell, J., Kamenov, G., Maclachlan, S., Rothwell, G., 2013. Response of Iberian Margin sediments to orbital and suborbital forcing over the past 420 ka. Paleoceanography 28, 185–199. https://doi.org/10.1002/palo.20017.

Hubbard, S.M., Covault, J.A., Fildani, A., Romans, B.W., 2014. Sediment transfer and deposition in slope channels: deciphering the record of enigmatic deep-sea processes from outcrop. Geol. Soc. Am. Bull. 126, 857–871. https://doi.org/10.1130/B30996.1.

Ito, T., Woloszyn, M., Mazloff, M., 2010. Anthropogenic carbon dioxide transport in the Southern Ocean driven by Ekman flow. Nature 463, 80–83. https://doi.org/10.1038/nature08687.

Iwai, M., Acton, G.D., Lazarus, D., Osterman, L.E., Williams, T., 2002. Magnetobiochronologic synthesis of ODP Leg 178 rise sediments from the Pacific sector of the Southern Ocean: Sites1095, 1096, and 1101. In: Barker, P.F., Camerlenghi, A., Acton, G.D., Ramsay, A.T.S. (Eds.), Proceedings of Ocean Drilling Program, Sci. Res, vol. 178, pp. 1–40. https://doi.org/10.2973/odp.proc.sr.178.236.2002.

Jiménez-Espejo, F.J., Presti, M., Kuhn, G., Mckay, R., Crosta, X., Escutia, C., Lucchi, R.G., Tolotti, R., Yoshimura, T., Huertas, M.O., Macrì, P., Caburlotto, A., De Santis, L., 2020. Late Pleistocene oceanographic and depositional variations along the Wilkes Land margin (East Antarctica) reconstructed with geochemical proxies in deep-sea sediments. Glob. Planet. Chang. 184, 103045 https://doi.org/10.1016/j.gloplacha.2019.103045.

Jin, Y.K., Larter, R.D., Kim, Y., Nam, S.H., Kim, K.J., 2002. Post-subduction margin structures along Boyd Strait, Antarctic Peninsula. Tectonophysics 346, 187–200. https://doi.org/10.1016/S0040-1951(01)00281-5.

Kemp, A.E.S., Grigorov, I., Pearce, R.B., Naveira Garabato, A.C., 2010. Migration of the Antarctic Polar Front through the mid-Pleistocene transition: evidence and climatic implications. Quat. Sci. Rev. 29, 1993–2009. https://doi.org/10.1016/j.quascirev.2010.04.027.

Kuijpers, A., Troelstra, S.R., Prins, M.A., Linthout, K., Akhmetzhanov, A., Bouryak, S., Bachmann, M.F., Lassen, S., Rasmussen, S., Jensen, J.B., 2003. Late Quaternary sedimentary processes and ocean circulation changes at the Southeast Greenland margin. Mar. Geol. 195, 109–129. https://doi.org/10.1016/S0025-3227(02)00684-9.

Larter, R.D., Barker, P.F., 1989. Seismic stratigraphy of the Antarctic Peninsula Pacific margin: a record of Pliocene–Pleistocene ice volume and paleoclimate. Geology 17, 731–734. https://doi.org/10.1130/0091-7613(1989)017<0731:SSOTAP>2.3.CO;2.

Larter, R.D., Barker, P.F., 1991a. Neogene interaction of tectonic and glacial processes at the Pacific margin on the Antarctic Peninsula. In: Macdonald, D.I.M. (Ed.), Sedimentation, Tectonics and Eustasy, 12. International Association of Sedimentologists, Blackwell, Oxford, pp. 165–186. https://doi.org/10.1002/9781444303896.ch10. Spec. Publ.

Larter, R.D., Barker, P.F., 1991b. Effects of ridge crest-trench interaction on Antarctic-Phoenix spreading: forces on a young subducting plate. J. Geophys. Res. 96, 583–607. https://doi.org/10.1029/91JB02053.

Larter, R.D., Cunningham, A.P., 1993. The depositional pattern and distribution of glacial-interglacial sequences on the Antarctic Peninsula Pacific margin. Mar. Geol. 109, 203–219. https://doi.org/10.1016/0025-3227(93)90061-Y.

Larter, R.D., Rebesco, M., Vanneste, L.E., Gambôa, L.A.P., Barker, P.F., 1997. Cenozoic tectonic, sedimentary and glacial history of the continental shelf west of Graham Land, Antarctic Peninsula. In: Barker, P.F., Cooper, A.K. (Eds.), Geology and Seismic Stratigraphy of the Antarctic Margin, 2, American Geophysical Union, Washington DC, Ant. Res. Series, vol. 71, pp. 1–27. https://doi.org/10.1029/AR071p0001.

Larter, R.D., Hogan, K.A., Hillenbrand, C.-D., Smith, J.A., Batchelor, C.L., Cartigny, M., Tate, A.J., Kirkham, J.D., Roseby, Z.A., Kuhn, G., Graham, A., Dowdeswell, J.A., 2019. Subglacial hydrological control on flow of an Antarctic Peninsula palaeo-ice stream. Cryosphere 13, 1583–1596. https://doi.org/10.5194/tc-13-1583-2019.

Larter, E., Hogan, K., Hillenbrand, C.-D., Gowland, E., 2021. Topographic Parametric Sonar (TOPAS) Acoustic Sub-Bottom Profiler Data Acquired on RRS James Clark Ross JR298 Cruise in 2015. Version 1.0. NERC EDS UK Polar Data Centre. https://doi.org/10.5285/BDFEB69C-DF5C-461D-B7A8-583F9DAAB685.

Laskar, J., Robutel, P., Joutel, F., Gastineau, M., Correia, A.C.M., Levrard, B., 2004. A long-term numerical solution for the insolation quantities of the Earth. Celest. Mech. Astro 428, 261–285. https://doi.org/10.1051/0004-6361:20041335.

Laskar, J., Fienga, A., Gastineau, M., Manche, H., 2011. La2010: a new orbital solution for the long-term motion of the Earth. Astron. Astrophys. 532, 1–15. https://doi.org/10.1051/0004-6361/201116836.

Lauer-Leredde, C., Briqueu, L., Williams, T., 2002. A Wavelet Analysis of Physical Properties measured Downhole and on Core from Holes 1095B and 1096C (Antarctic Peninsula). In: Barker, P.F., Camerlenghi, A., Acton, G.D., Ramsay, A.T.S. (Eds.), Proceedings of the Ocean Drilling Program, ODP, Sci. Res, vol. 178, pp. 1–43. https://doi.org/10.2973/odp.proc.sr.178.205.2001.

Lavoie, C., Domack, E.W., Pettit, E.C., Scambos, T.A., Larter, R.D., Schenke, H.-W., Yoo, K.C., Gutt, J., Wellner, J., Canals, M., Anderson, J.B., Amblas, D., 2015. Configuration of the Northern Antarctic Peninsula Ice Sheet at LGM based on a new synthesis of seabed imagery. Cryosphere 9 (613–629), 2015. https://doi.org/10.5194/tc-9-613-2015.

Levin, L.A., Bett, B.J., Gates, A.R., Heimbach, P., Howe, B.M., Janssen, F., McCurdy, A., Ruhl, H.A., Snelgrove, P., Stocks, K.I., Bailey, D., Baumann-Pickering, S., Beaverson, C., Benfield, M.C., Booth, D.J., Carreiro-Silva, M., Colaco, A., Eblé, M.C., Fowler, A.M., Gjerde, K.M., Jones, D.O.B., Katsumata, K., Kelley, D., Le Bris, N., Leonardi, A.P., Lejzerowicz, F., Macreadie, P.I., McLean, D., Meitz, F., Morato, T., Netburn, A., Pawlowski, J., Smith, C.R., Sun, S., Uchida, H., Vardaro, M.F., Venkatesan, R., Weller, R.A., 2019. Global observing needs in the deep ocean. Front. Mar. Sci. 6 https://doi.org/10.3389/fmars.2019.00241, 32 pp.

Lisiecki, L., 2005. A Pliocene-Pleistocene stack of 57 globally distributed benthic $\delta^{18}O$ records. Paleoceanography 20. https://doi.org/10.1029/2004PA001071.

Liu, L., Tingshan, Z., Xiaoming, Z., Shenghe, W., Jialiang, H., Xing, W., Yikai, Z., 2013. Sedimentary architecture models of deepwater turbidite channel systems in the Niger Delta continental slope, West Africa. Pet. Sci. 10, 139–148. https://doi.org/10.1007/s12182-013-0261-x.

Liu, Q., Kneller, B., Fallgatter, C., Buso, V.V., 2018. Quantitative comparisons of depositional architectures of unconfined and confined turbidite sheet systems. Sediment. Geol. 376, 72–89. https://doi.org/10.1016/j.sedgeo.2018.08.005.

Livingstone, S.J., Ó Cofaigh, C., Stokes, C.R., Hillenbrand, C.-D., Vieli, A., Jamieson, S.S. R., 2013. Glacial geomorphology of Marguerite Bay Palaeo-Ice stream, western Antarctic Peninsula. J. Maps 9, 558–572. https://doi.org/10.1080/17445647.2013.829411.

Lucchi, R.G., Rebesco, M., 2007. Glacial contourites on the Antarctic Peninsula margin: Insight for palaeoenvironmental and palaeoclimatic conditions. In: Viana, A.R., Rebesco, M. (Eds.), Economic and Palaeoceanographic Significance of Contourite Deposits, Geol. Soc. London Spec. Publ, vol. 276, pp. 111–127. https://doi.org/10.1144/GSL.SP.2007.276.01.06.

Lucchi, R.G., Rebesco, M., Camerlenghi, A., Busetti, M., Tomadin, L., Villa, G., Persico, D., Morigi, C., Bonci, M.C., Giorgetti, G., 2002. Mid-late Pleistocene glacimarine sedimentary processes of a high-latitude, deep-sea sediment drift (Antarctic Peninsula Pacific margin). Mar. Geol. 189, 343–370. https://doi.org/10.1016/S0025-3227(02)00470-X.

Lucchi, R.G., Camerlenghi, A., Rebesco, M., Colmenero-Hidalgo, E., Sierro, F.J., Sagnotti, L., Urgeles, R., Melis, R., Morigi, C., Barcena, M.-A., Giorgetti, G., Villa, G., Persico, D., Flores, J.-A., Rigual-Hernandez, A.S., Pedrosa, M.T., Macrì, P., Caburlotto, A., 2013. Postglacial sedimentary processes on the Storfjorden and Kveithola trough mouth fans: significance of extreme glacimarine sedimentation. Glob. Planet. Chang. 111, 309–326. https://doi.org/10.1016/j.gloplacha.2013.10.008.

Macrì, P., Sagnotti, L., Lucchi, R.G., Rebesco, M., 2006. A stacked record of relative geomagnetic paleointensity for the past 270 kyr from the western continental rise of the Antarctic Peninsula. Earth Planet. Sci. Lett. 252, 162–179. https://doi.org/10.1016/j.epsl.2006.09.037.

Maslin, M.A., Ridgwell, A.J., 2005. Mid-Pleistocene revolution and the 'eccentricity myth'. In: Head, M.J., Gibbard, P.L. (Eds.), Early–Middle Pleistocene Transitions: The Land–Ocean Evidence, Geol. Soc. London Spec. Publ, vol. 247, pp. 19–34. https://doi.org/10.1144/GSL.SP.2005.247.01.02.

McCave, I.N., 2008. Size sorting during transport and deposition of fine sediments: Sortable silt and flow speed. In: Rebesco, M., Camerlenghi, A. (Eds.), Contourites. Dev. Sedimentol, p. 60. https://doi.org/10.1016/S0070-4571(08)10008-5.

McCave, I.N., Thornalley, D.J.R., Hall, I.R., 2017. Relation of sortable silt grain-size to deep-sea current speeds: Calibration of the 'Mud Current Meter'. In: Deep Sea Res. Part I: Oceanogr. Res. Papers, 127, pp. 1–12. https://doi.org/10.1016/j.dsr.2017.07.003.

McClymont, E.L., Sosdian, S.M., Rosell-Melé, A., Rosenathal, Y., 2013. Pleistocene sea surface temperature evolution: early cooling, delayed glacial intensification, and implications for the mid-Pleistocene climate transition. Earth Sci. Rev. 123, 173–193. https://doi.org/10.1016/j.earscirev.2013.04.006.

McGinnis, J.P., Hayes, D.E., 1995. The roles of down-slope and along-slope depositional processes: Southern Antarctic Peninsula continental rise. In: Cooper, A.K., Barker, P. F., Brancolini, G. (Eds.), Geology and Seismic Stratigraphy of the Antarctic Margin, American Geophysical Union, Washington DC, Ant. Res. Series, vol. 68, pp. 141–156. https://doi.org/10.1029/AR068p0141.

McGinnis, J.P., Hayes, D.E., Driscoll, N.W., 1997. Sedimentary processes across the continental rise of the southern Antarctic Peninsula. Mar. Geol. 141, 91–109. https://doi.org/10.1016/S0025-3227(97)00056-X.

Mencaroni, D., Urgeles, R., Camerlenghi, A., Llopart, J., Ford, J., Serra, C.S., Meservy, W., Gràcia, E., Rebesco, M., Zitellini, N., 2021. A mixed turbidite – contourite system related to a major submarine canyon: the Marquês de Pombal Drift (south-west Iberian margin). Sedimentology. https://doi.org/10.1111/sed.12844 (in press).

Michels, K.H., Rogenhagen, J., Kuhn, G., 2001. Recognition of contour-current influence in mixed contourite-turbidite sequences of the western Weddell Sea, Antarctica. Mar. Geophys. Res. 22, 465–485. https://doi.org/10.1023/A:1016301817273.

Miller, K.G., Kominz, M.A., Browning, J.V., Wright, J.D., Mountain, G.S., Katz, M.E., Sugarman, P.J., Cramer, B.S., Christie-Blick, N., Pekar, S.F., 2005. The phanerozoic record of global sea-level change. Science 310, 1293–1298. https://doi.org/10.1126/science.1116412.

Miller, K.G., Mountain, G.S., Wright, J.D., Browning, J.V., 2011. A 180-million-year record of sea level and ice volume variations from continental margin and deep-sea isotopic records. Oceanography 24, 40–53. https://doi.org/10.5670/oceanog.2011.26.

Miramontes, E., Eggenhuisen, J.T., Jacinto, R.S., Poneti, G., Pohl, F., Normndeau, A., Campbell, D.C., Hernández-Molina, F.J., 2020. Channel-levee evolution in combined contour current–turbidity current flows from flume-tank experiments. Geology 48, 353–357. https://doi.org/10.1130/G47111.1.

Miramontes, E., Thiéblemont, A., Babonneau, N., Penven, P., Raisson, F., Droz, L., Jorry, S.J., Fierens, R., Counts, J.W., Wilckens, H., Cattaneo, A., Jouet, G., 2021. Contourite and mixed turbidite-contourite systems in the Mozambique Channel (SW Indian Ocean): link between geometry, sediment characteristics and modelled bottom currents. Mar. Geol. https://doi.org/10.1016/j.margeo.2021.106502 (in press).

Mitchum, R.M., Vail, P.R., Sangree, J.B., 1977. Seismic stratigraphy and global changes of sea level, part 6: Stratigraphic interpretation of seismic reflection patterns in depositional sequences. In: Payton, C.E. (Ed.), Seismic Stratigraphy – Applications to Hydrocarbon Exploration, vol. 26. AAPG Mem, pp. 117–133.

Mosher, D.C., Campbell, D.C., Gardner, J.V., Piper, D.J.W., Chaytor, J.D., Rebesco, M., 2017. The role of deep-water sedimentary processes in shaping a continental margin: the Northwest Atlantic. Mar. Geol. 393, 245–259. https://doi.org/10.1016/j.margeo.2017.08.018.

Mulder, T., Faugères, J.-C., Gonthier, E., 2008. Mixed turbidite-contourite systems. In: Rebesco, M., Camerlenghi, A. (Eds.), Contourites. Dev. Sedimentol, 60. Elsevier, Amsterdam, pp. 435–456. https://doi.org/10.1016/S0070-4571(08)10021-8.

Mutti, E., Normark, W., 1987. Comparing examples of modern and ancient turbiite systems: Problems and concepts. In: Leggett, J.K., Zuffa, G.G. (Eds.), Marine Clastic Sedimentology: Concepts and Case Studies. Graham & Trotman, London, pp. 1–38.

Mutti, E., Bernoulli, D., Ricci Lucchi, F., Tinterri, R., 2009. Turbidites and turbidity currents from Alpine "Flysch" to the exploration of continental margins. In: McKenzie, J.A., Bernoulli, D., Cita, M.B. (Eds.), Symposium on Major Discoveries in Sedimentary Geology in the Mediterranean Realm from a Historical Perspective to New Development, Sedimentology, vol. 56, pp. 267–318. https://doi.org/10.1111/j.1365-3091.2008.01019.x.

Mutti, E., Cunha, R.S., Bulhoes, E.M., Arienti, L.M., Viana, A.R., 2014. Contourites and Turbidites of the Brazilian Marginal Basins. Search Disc. Art. #51069.

Naish, T., Carter, L., Wolff, E., Pollard, D., Powell, R., 2009. Chapter 11 Late Pliocene-Pleistocene Antarctic climate variability at orbital and suborbital scale: Ice Sheet, ocean and atmospheric interactions. In: Florindo, F., Siegert, M. (Eds.), Developments in Earth and Environmental Sciences, 8. Elsevier, Amsterdam, pp. 465–529. https://doi.org/10.1016/S1571-9197(08)00011-6.

Naveira Garabato, A.C., Heywood, K.J., Stevens, D.P., 2002. Modification and pathways of southern ocean deep waters in the Scotia Sea. Deep-Sea Res. I 49, 681–705. https://doi.org/10.1016/S0967-0637(01)00071-1.

Naveira Garabato, A.C., Stevens, D.P., Heywood, K.J., 2003. Water mass convection, fluxes and mixing in the Scotia Sea diagnosed by an inverse model. J. Phys. Oceanogr. 33, 2565–2587. https://doi.org/10.1175/1520-0485(2003)033<2565:WMCFAM>2.0.CO;2.

Nerlich, R., Clark, S.R., Bunge, H.-P., 2013. The Scotia Sea gateway: no outlet for Pacific mantle. Tectonophysics 604, 41–50. https://doi.org/10.1016/j.tecto.2012.08.023.

Nowlin Jr., W.D., Zenk, W., 1988. Westward bottom currents along the margin of the South Shetland Island Arc. Deep-Sea Res. 35, 269–301. https://doi.org/10.1016/0198-0149(88)90040-4.

Ó Cofaigh, C., Pudsey, C.J., Dowdeswell, J.A., Morris, P., 2002. Evolution of subglacial bedforms along a paleo-ice stream, Antarctic Peninsula continental shelf. Geophys. Res. Lett. 29 https://doi.org/10.1029/2001GL014488.

Ogg, J.G., Ogg, G.M., Gradstein, F.M., Gradstein, F.M., 2016. 16 – Quaternary. In: Ogg, J. G., Ogg, G.M. (Eds.), A Concise Geologic Time Scale. Elsevier, pp. 211–226. https://doi.org/10.1016/B978-0-444-59467-9.00016-9.

Orsi, A.H., Whitworth III, T., Nowlin Jr., W.D., 1995. On the meridional extent and fronts of the Antarctic circumpolar current. Deep-Sea Res. I 42, 641–673. https://doi.org/10.1016/0967-0637(95)00021-W.

Orsi, A.H., Johnson, G.C., Bullister, J.L., 1999. Circulation, mixing, and production of Antarctic bottom water. Prog. Oceanogr. 43, 55–109. https://doi.org/10.1016/S0079-6611(99)00004-X.

Palmer, M., Gomis, D., Flexas, M.D.M., Jordà, G., Jullion, L., Tsubouchi, T., Naveira-Garabato, A.C., 2012. Water mass pathways and transports over the South Scotia Ridge west of 50°W. Deep-Sea Res. I 59, 8–24. https://doi.org/10.1016/j.dsr.2011.10.005.

Pandolpho, B.T., Klein, A.H., Dutra, I., Mahiques, M.M., Viana, A.R., Bueno, G.V., Machado, A.A., Camargo, Y.L., Hercos, C.M., Lima, Y., Filho, A.F., Theodoro, C.E., 2021. Seismic record of a cyclic turbidite-contourite system in the Northern Campos Basin, SE Brazil. Mar. Geol. 434, 106422 https://doi.org/10.1016/j.margeo.2021.106422.

Patterson, S.L., Whitworth, T., 1989. Physical oceanography. In: Glasby, G.P. (Ed.), Antarctic Sector of the Pacific, Elsevier Oceanogr. Series, vol. 51. Elsevier, Amsterdam, pp. 55–93. https://doi.org/10.1016/S0422-9894(08)70517-8.

Poblete, E., Arriagada, C., Roperch, P., Astudillo, N., Hervé, F., Kraus, S., Le Roux, J.P., 2011. Paleomagnetism and tectonics of the South Shetland Islands and the northern Antarctic Peninsula. Earth Planet. Sci. Lett. 302, 299–313. https://doi.org/10.1016/j.epsl.2010.12.019.

Postma, G., Cartigny, M.B., Kleverlaan, K., 2009. Structureless, coarse-tail graded Bouma Ta formed by internal hydraulic jump of the turbidity current? Sediment. Geol. 219, 1–6. https://doi.org/10.1016/j.sedgeo.2009.05.018.

Pudsey, C.J., 2000. Sedimentation on the continental rise west of the Antarctic Peninsula over the last three glacial cycles. Mar. Geol. 167, 313–338. https://doi.org/10.1016/S0025-3227(00)00039-6.

Pudsey, C.J., 2002. Neogene record of Antarctic Peninsula glaciation in continental rise sediments: ODP Leg 178, Site 1095. In: Barker, P.F., Camerlenghi, A., Acton, G.D., Ramsay, A.T.S. (Eds.), ODP Proceedings, Sci. Res, vol. 178, pp. 1–25. https://doi.org/10.2973/odp.proc.sr.178.214.2001.

Pudsey, C.J., Camerlenghi, A., 1998. Glacial-interglacial deposition on a sediment drift on the Pacific margin of the Antarctic Peninsula. Antarct. Sci. 10, 286–308. https://doi.org/10.1017/S0954102098000376.

Rasmussen, S.L., Lykke-Andersen, H., Kuijpers, A., Troelstra, S.R., 2003. Post-miocene sedimentation at the continental rise of Southeast Greenland: the interplay between turbidity and contour currents. Mar. Geol. 196, 37–52. https://doi.org/10.1016/S0025-3227(03)00043-4.

Rea, D.K., Moore, T.C., Hassold, N., van der Pluijm, B., 2016. Do magnetic fabrics of marine deposits preserve orbital forcing? A test case in the Southern Ocean, Antarctic Peninsula. Lithosphere 8 (6), 751–756. https://doi.org/10.1130/L566.1.

Rebesco, M., Camerlenghi, A., 2008. Late Pliocene margin development and mega debris flow deposits on the Antarctic continental margins: evidence of the onset of the modern Antarctic Ice Sheet? Palaeogeogr. Palaeoclimatol. Palaeoecol. 260, 149–167. https://doi.org/10.1016/j.palaeo.2007.08.009.

Rebesco, M., Larter, R.D., Camerlenghi, A., Barker, P.F., 1996. Giant sediment drifts on the continental rise west of the Antarctic Peninsula. Geo-Mar. Lett. 16, 65–75. https://doi.org/10.1007/BF02202600.

Rebesco, M., Larter, R.D., Barker, P.F., Camerlenghi, A., Vanneste, L.E., 1997. The history of sedimentation on the continental rise west of the Antarctic peninsula. In: Cooper, A.K., Barker, P.F. (Eds.), Geology and Seismic Stratigraphy of the Antarctic Margin II, pp. 28–49. https://doi.org/10.1029/AR071p0029. AGU Ant. Res. Series 0066–4634, 71, 0–87590–884-5.

Rebesco, M., Camerlenghi, A., Zanolla, C., 1998. Bathymetry and morphogenesis of the continental margin west of the Antarctic Peninsula. Terra Antart. 5, 715–725.

Rebesco, M., Pudsey, C., Canals, M., Camerlenghi, A., Barker, P., Estrada, F., Giorgetti, A., 2002. Sediment drift and deep-sea channel systems, Antarctic Peninsula Pacific margin. In: Stow, D.A.V., Pudsey, C.J., Howe, J.A., Faugères, J.C., Viana, A.R. (Eds.), Deep-Water Contourite Systems: Modern Drifts and Ancient Series, Seismic and Sedimentary Characteristics, Geol. Soc. London Mem, vol. 22, pp. 353–371. https://doi.org/10.1144/GSL.MEM.2002.022.01.25.

Rebesco, M., Camerlenghi, A., Volpi, V., Neagu, C., Accettella, D., Lindberg, B., Cova, A., Zgur, F., the MAGICO party, 2007. Interaction of processes and importance of contourites: Insights from the detailed morphology of sediment drift 7, Antarctica. In: Viana, A.R., Rebesco, M. (Eds.), Economic and Palaeoceanographic Significance of Contourite Deposits, Geol. Soc. London Spec. Publ, vol. 276, pp. 95–110. https://doi.org/10.1144/GSL.SP.2007.276.01.05.

Rebesco, M., Hernández-Molina, F.J., Van Rooij, D., Wåhlin, A., 2014. Contourites and associated sediments controlled by deep-water circulation processes: state-of-the-art and future considerations. Mar. Geol. 352, 111–154. https://doi.org/10.1016/j.margeo.2014.03.011.

Rodrigues, S., Hernández-Molina, F.J., Kirby, A., 2021. Late Cretaceous hybrid (turbidite-contourite) system along the Argentine Margin: paleoceanographic and conceptual implications. Mar. Pet. Geol. 104768 https://doi.org/10.1016/j.marpetgeo.2020.104768.

Sagnotti, L.P., Macrì, P., Camerlenghi, A., Rebesco, M., 2001. Environmental magnetism of late Pleistocene sediments from the Pacific margin of the Antarctic Peninsula and interhemispheric correlation of climatic events. Earth Planet. Sci. Lett. 192, 65–80. https://doi.org/10.1016/S0012-821X(01)00438-1.

Salabarnada, A., Escutia, C., Röhl, U., Hans Nelson, C., McKay, R., Jiménez-Espejo, F.J., Bijl, P.K., Hartman, J.D., Strother, S.L., Salzmann, U., Evangelinos, D., López-Quirós, A., Flores, J.A., Sangiorgi, F., Ikehara, M., Brinkhuis, H., 2018. Paleoceanography and ice sheet variability offshore Wilkes Land, Antarctica – part 1: insights from late Oligocene astronomically paced contourite sedimentation. Clim. Past 14, 991–1014. https://doi.org/10.5194/cp-14-991-2018.

Sansom, P., 2017. Turbidites v Contourites: Hybrid systems of the Tanazanian margin. In: Extended Abstract, PESGB/HGS African Conference, London.

Sansom, P., 2018. Hybrid turbidite-contourite systems of the Tanzanian margin. Geol. Soc. Lond. Petrol. Geosci. 24, 258–276. https://doi.org/10.1144/petgeo2018-044.

Scheuer, C., Gohl, K., Larter, R.D., Rebesco, M., Udintsev, G., 2006. Variability in Cenozoic sedimentation along the continental rise of the Bellingshausen Sea, West Antarctica. Mar. Geol. 277, 279–298. https://doi.org/10.1016/j.margeo.2005.12.007.

Shanmugam, G., 2016. Slides, slumps, debris flows, turbidity currents, and bottom currents. In: Reference Module in Earth Systems and Environmental Sciences, 4. Elsevier, Amsterdam, Netherlands. https://doi.org/10.1016/B978-0-12-409548-9.04380-3.

Shanmugam, G., Spalding, T.D., Rofheart, D.H., 1993. Process sedimentology and reservoir quality of deep-marine bottom current reworked sands (sandy contourites), an example from the Gulf of Mexico. AAPG Bull. 77, 1241–1259. https://doi.org/10.1306/BDFF8E52-1718-11D2-8645000102C1865D.

Solheim, A., Andersen, E.S., Elverhøi, A., Fiedler, A., 1996. Late Cenozoic depositional history of the western Svalbard continental shelf, controlled by subsidence and climate. Glob. Planet. Chang. 12, 135–148. https://doi.org/10.1016/0921-8181(95)00016-X.

Thunell, R., Rio, D., Sprovieri, R., Vergnaud-Grazzini, C., 1991. An overview of the post-Messinian paleoenvironmental history of the Mediterranean. Paleoceanography 6, 143–164. https://doi.org/10.1029/90PA02339.

Tucholke, B.E., 1977. Sedimentation processes and acoustic stratigraphy in the Bellingshausen Basin. Mar. Geol. 25, 209–230. https://doi.org/10.1016/0025-3227(77)90053-6.

Tucholke, B.E., Houtz, R.E., 1976. Sedimentary framework of the Bellingshausen basin from seismic profiler data. Init. Rep. DSDP 35, 197–228. https://doi.org/10.2973/dsdp.proc.35.107.1976.

Uenzelmann-Neben, G., 2006. Depositional patterns at Drift 7, Antarctic Peninsula: along-slope versus down-slope sediment transport as indicators for oceanic currents and climatic conditions. Mar. Geol. 233, 49–62. https://doi.org/10.1016/j.margeo.2006.08.008.

Vautravers, M.J., Hodell, D.A., Channell, J., Hillenbrand, C.-D., Hall, M., Smith, J., Larter, R.D., 2013. Palaeoenvironmental records from the West Antarctic Peninsula drift sediments over the last 75. In: Hambrey, M.J., Barker, P.F., Barrett, P.J., Bowman, V., Davies, B., Smellie, J.L., Tranter, M. (Eds.), Antarctic Palaeoenvironments and Earth-Surface Processes, Geol. Soc. London Spec. Publ, vol. 381, pp. 263–276. https://doi.org/10.1144/SP381.12.

Venuti, A., Florindo, F., Caburlotto, A., Hounslow, M.W., Hillenbrand, C.-D., Strada, E., Talarico, F.M., Cavallo, A., 2011. Late Quaternary sediments from deep-sea sediment drifts on the Antarctic Peninsula Pacific margin: climatic control on provenance of minerals. J. Geophys. Res. 116, B06104. https://doi.org/10.1029/2010JB007952.

Viana, A.R., Faugères, J.-C., Stow, D.A.V., 1998. Bottom current controlled sand deposits – a review of modern shallow- to deep-water environments. Sediment. Geol. 115, 53–80. https://doi.org/10.1016/S0037-0738(97)00087-0.

Villa, G., Persico, D., Bonci, M.C., Lucchi, R.G., Morigi, C., Rebesco, M., 2003. Biostratigraphic characterization and Quaternary microfossil palaeoecology in sediment drifts west of the Antarctic Peninsula – implications for cyclic glacial-interglacial deposition. Palaeogeogr. Palaeoclimatol. Palaeoecol. 198 https://doi.org/10.1016/S0031-0182(03)00403-6, 273–263.

Volpi, V., Camerlenghi, A., Moerz, T., Corubolo, P., Rebesco, M., Tinivella, U., 2001. Data report: Physical properties relevant to seismic stratigraphic studies, Continental Rise Sites 1095, 1096, and 1101, ODP Leg 178, Antarctic Peninsula. In: Barker, P.F., Camerlenghi, A., Acton, G.D., Ramsay, A.T.S. (Eds.), Proceedings of the Ocean Drilling Program, ODP, Sci. Res, vol. 178, pp. 1–36. https://doi.org/10.2973/odp.proc.sr.178.228.2001.

Volpi, A., Florindo, F., Caburlotto, A., Hounslow, M.W., Hillenbrand, C.-D., Strada, E., Talarico, F.M., Cavallo, A., 2011. Late Quaternary sediments from deep-sea sediment drifts on the Antarctic Peninsula Pacific margin: climatic control on provenance of minerals. J. Geophys. Res. 116, 1–18. https://doi.org/10.1029/2010JB007952.

Wright, R., Anderson, J.B., 1982. The importance of sediment gravity flow to sediment transport and sorting in a glacial marine environment: Eastern Scotia Sea. GSA Bull. 93 (10), 951–963. https://doi.org/10.1130/0016-7606(1982)93<951:TIOSGF>2.0.CO;2.

Yegorova, T., Bakhmutov, V., 2013. Crustal structure of the Antarctic Peninsula sectors of the Gondwana margin around Anvers Island from geophysical data. Tectonophysics 585, 77–89. https://doi.org/10.1016/j.tecto.2012.09.029.

Zecchin, M., Catuneanu, O., Rebesco, M., 2015. High-resolution sequence stratigraphy of clastic shelves IV: high-latitude settings. Mar. Petrol. Geo. 68, 427–437. https://doi.org/10.1016/j.marpetgeo.2015.09.004.